AIMS Energy, 13(5): 1012–1051.
DOI: 10.3934/energy.2025038
Received: 25 June 2025
Revised: 28 August 2025
Accepted: 02 September 2025
Published: 08 September 2025

https://www.aimspress.com/journal/energy

Research article

Multi-objective optimization using MISOCP model for service restoration in electrical distribution grids in the presence of distributed generation and voltage-dependent loads

Nang-Van Pham*, Trong-Sang Vo, Trung-Hai Nguyen and Dinh-Phu Vu

School of Electrical and Electronic Engineering, Hanoi University of Science and Technology, Hanoi, Vietnam

* **Correspondence:** Email: van.phamnang@hust.edu.vn.

Abstract: In this study, we present a multi-objective optimization framework formulated as mixed-integer second-order cone programming (MISOCP) to restore electricity distribution systems following fault clearance. The proposed model incorporated two objective functions: Minimizing the total unserved load while considering load prioritization and reducing the frequency of switching actions of sectionalizing devices. The model's constraints included preserving the radial configuration of the reconfigured distribution grid, power flow equations, PV models of distributed energy resources, voltage-dependent load models, node voltage limits, and branch power flow limits. The presented optimization framework was converted from the optimization model formulated as mixed-integer nonlinear programming (MINLP), achieved through the reformulation of nodal power balance equations as second-order cone constraints and the approximate formulation of the voltage-dependent load models for conic solvers. Pareto optimal solutions were then achieved through a heuristic approach. The proposed optimization framework was validated on the enhanced IEEE 33-node test feeder and a Vietnamese real 190-bus distribution grid, utilizing the CPLEX solver under the GAMS programming language. We also explored various fault location scenarios across the distribution grid and evaluated the influence of the different objective functions, as well as two load models, on the optimization outcomes.

Keywords: service restoration; power distribution grids; optimal Pareto front; second-order conic programming with integer variables (MISOCP); nonlinear programming with integer variables (MINLP)

Nomenclature: *Sets*: Ω_{N}: Collection of all nodes within the electrical distribution grid; Ω_{ope}: Set of branches that are initially open; Ω_{clo}: Set of branches that are initially closed; Ω_{L}: Collection of all branches within the power distribution network; Ω_{sub}: Collection of all substation buses; $\Omega_{\mathrm{N(i)}}$: Collection of nodes immediately adjacent to node *i* within the power grid; Ω_{DG}: Collection of nodes with DG in the power grid; Ω_{D}: Collection of nodes with load in the power grid;

Parameters: $P_{l1,i}, P_{l2,i}, P_{l3,i}$: The load power consumption at node *i* belonging to priority groups 1, 2, and 3; w_{l1}, w_{l2}, w_{l3}: The weighting factors corresponding to load priority groups 1, 2, and 3; ΔU_i: Node *i*'s voltage deviation from its nominal voltage; $U_{0,i}$: The target voltage at bus *i* in PV model of DG; $U_i^{\max}, U_i^{\min}$: The upper and lower bounds of voltage magnitude values at bus *i*; P_{DGi}: The active power output of the DG at bus *i*; $Q_{DGi}^{\max}, Q_{DGi}^{\min}$: The maximum and minimum reactive power outputs of the DG at bus *i*; $\begin{matrix}\cos\varphi_{i,lagging},\\ \cos\varphi_{i,leading}\end{matrix}$: The lagging and leading power factors of the DG at bus *i* when modeled as a PV node; $P_{\mathrm{D}i}, Q_{\mathrm{D}i}$: The active and reactive power consumption of loads at node *i*; R_{ij}, X_{ij}: The resistive and reactive components of branch *ij*; M: A large enough positive value (in this research, *M* is set to 20); $S_{ij}^{\max}$: The maximum permissible apparent power flows on the branch *ij*; $\begin{matrix}a_i^{\mathrm{P}}, b_i^{\mathrm{P}}, c_i^{\mathrm{P}},\\ a_i^{\mathrm{Q}}, b_i^{\mathrm{Q}}, c_i^{\mathrm{Q}}\end{matrix}$: The coefficients for the ZIP load model at node *i*; $P_{\mathrm{D0}i}, Q_{\mathrm{D0}i}$: The real power and reactive power of the load at bus *i* at the nominal voltage;

Variables: y_i: A binary variable representing the condition of bus *i* ($y_i = 1$ if bus *i* is energized, and $y_i = 0$ conversely); x_{ij}: A binary variable indicating the operational status of the branch ij ($x_{ij} = 1$ if the line section ij is supplied with power, and $x_{ij} = 0$ otherwise); γ_{ij}: A binary variable ($\gamma_{ij} = 1$ if the line section ij is not supplied with power, and its sectionalizing switch is reclosed following network restoration, and $\gamma_{ij} = 0$ conversely); k_{ij}: A binary variable representing the direction of power flow on the branch ij ($k_{ij} = 1$ when node j receives power from the node i, and $k_{ji} = 1$ reveals an inverse direction); $k_{sub,j}$: A binary variable representing the direction of power flow on the branch with a substation; $\beta_i^{\min}, \beta_i^{\max}$: The binary variables representing the reactive power generation state of the DG at node *i* ($\beta_i^{\min} = 1$ if the reactive power of the DG reaches its minimum value, $\beta_i^{\max} = 1$ if the reactive power of the DG reaches its maximum value, $\beta_i^{\min} = \beta_i^{\max} = 0$ if the reactive power of the DG is within the allowable range); d_i: An auxiliary variable; U_i: The voltage magnitude at node *i*; Q_{DGi}: The reactive power output of the DG at bus *i*; P_{ij}, Q_{ij}: The real power and reactive power flows on the branch *ij*; $P_{\mathrm{G}i}, Q_{\mathrm{G}i}$: The active and reactive power injection of generators at node

i; V_i: Square of the voltage magnitude at node i; I_{ki}: Square of the current magnitude in the branch ij; f_1: Sub-objective of post-restoration unserved load minimization; f_2: Sub-objective of switching operation minimization

1. Introduction

1.1. Motivation and background

As the demand for electric power surges, so does the scale and intricacy of contemporary distribution networks, directly correlating with a higher probability of faults. In reality, most power interruptions experienced by consumers can be traced back to failures within the distribution network. The economic and social impact of these supply interruptions is substantial for both providers and end-users. Consequently, to bolster the reliability of electricity provision and cultivate improved customer satisfaction, prioritizing a thorough investigation into power restoration techniques is essential.

Voltage is a crucial constraint in the service restoration problem. A solution may restore a significant amount of load, but if it fails to maintain voltage within permissible limits, that load cannot operate. Therefore, ignoring voltage constraints can lead to infeasible restoration solutions. In addition, many researchers exploring this topic [1, 2] have integrated voltage constraints into their optimization models, highlighting their importance.

The voltage-dependent load model is more realistic than the constant power load model, especially during severe voltage sags after a fault. For instance, a voltage-dependent model for commercial loads with specific coefficients [3] shows that at 0.9 p.u. voltage, the actual active and reactive powers differ by 11.04% and 30.94% from a constant power load model, respectively. Papers [4, 5] further emphasize the critical impact of the load model in power system studies. Thus, it is essential to investigate the influence of the load model in the service restoration problem.

In real-world applications, grid operators must also consider factors such as power loss and the number of switching operations, in addition to the total unserved load. A solution that focuses solely on maximizing load restoration may lead to very high energy losses or require an impractical number of switching operations, which increases costs and reduces the lifespan of equipment. Numerous studies, such as [1, 6] on service restoration, also entail multi-objective optimization. Therefore, using multiple objectives helps find a set of compromise solutions that balances load restoration, loss reduction, and the minimization of switching operations. This approach provides grid operators with a wider range of practical and optimal choices for decision-making.

1.2. Research literature

In recent years, significant attention has been given to multi-criteria optimization techniques to facilitate power recovery within electricity distribution networks, particularly in the context of distributed generation (DG) and voltage-dependent loads. The researchers in [7] reviewed recent advances and conceptual foundations of the processes of fault identification, isolation, and power restoration within electrical distribution networks, comparing approaches and practices. It also highlighted the technical, ecological, and financial obstacles associated with deploying self-healing power networks, concluding with recommendations for future research directions. The following studies provide a comprehensive foundation for understanding current modeling approaches and their

impact on grid reliability and performance.

Several researchers have explored the application of multi-objective evolutionary algorithms (MOEAs) as a robust approach to solving complex, multi-objective problems in power systems. The researchers in [8] investigated the use of Pareto-based evolutionary computation techniques for multi-objective evolutionary algorithms, such as nondominated sorting genetic algorithm (NSGA), niched Pareto genetic algorithm (NPGA), and strength Pareto evolutionary algorithm (SPEA), to address environmental and economic dispatch problems in power systems. To improve feasibility and decision-making, the authors incorporated constraint-handling techniques, hierarchical clustering for Pareto set reduction, and a fuzzy logic-driven approach for determining a compromise outcome. Their experiments on the IEEE 30-node test feeder showed that MOEAs, especially SPEA, outperformed traditional optimization methods in handling complex multi-objective tasks. The researchers in [9] quantitatively compared four multi-objective evolutionary algorithms (EAs) using a modified 0/1 knapsack problem utilized as a benchmark scenario. They proposed a new Strength Pareto Evolutionary Algorithm that integrated multiple functionalities from existing algorithms, such as external storage of nondominated solutions and clustering to maintain diversity. The results demonstrated that SPEA outperformed the other algorithms by effectively sampling the Pareto front and distributing solutions across the trade-off surface. Furthermore, the researchers in [10] developed an optimization model featuring both integer and continuous variables and linear constraints to optimize conductor sizing and reconductoring in radially configured distribution networks using linearized steady-state operation constraints. The proposed method, combined with a heuristic, was tested on both a benchmark system along two practical distribution grids, demonstrating accuracy and computational efficiency while generating the Pareto front for two objective functions.

Several researchers have focused on using robust optimization to address the uncertainties in service restoration. The researchers in [11] proposed a robust restoration decision-making model employing information gap theory to address imprecision in load demands and distributed generator outputs during service restoration. Implemented via an optimization problem with mixed-integer variables and quadratic constraints (MIQCP), the model was tested on the 69-node PG&E test system, demonstrating its ability to ensure feasibility and maximize restored loads under uncertain conditions. The researchers in [12] proposed a flexible, robust optimization model for service restoration, addressing uncertainties in distributed generation outputs and load demands through a two-stage approach involving recovery strategies and worst-case scenario analysis. Formulated as a linear program involving both integer and continuous variables (MILP) and addressed using column-and-constraint generation, the model underwent validation using adapted PG&E 69-node and 246-node networks, demonstrating superior feasibility and reliability compared to deterministic methods.

A wide range of optimization models has been developed to address the complex challenge of service restoration in modern distribution networks. The findings in [13] proposed a step-by-step service recovery process (SSR) framework to orchestrate the operation of switches, distributed generators, and loads for forming microgrids during large-scale outages. Formulated as a linear program involving both integer and continuous variables, the validation of the model was conducted on an adapted IEEE 123-bus test feeder and showed adaptability to various operating conditions in unbalanced systems. Moreover, the researchers in [14] developed a multi-period service recovery approach to optimize control sequences of switches, energy storage systems, and distributed generators under cold load pickup conditions. The method, formulated as a mixed-integer linear program, was

validated on modified IEEE 13-node and 123-node feeders, effectively minimizing unserved customers while respecting operational constraints. The findings in [15] proposed an optimization model formulated as an optimization problem with both integer and continuous variables and linear constraints, alongside a heuristic method to enhance the efficiency of service recovery within interconnected medium-voltage networks following main substation outages, aiming to reduce the average system interruption duration (SAIDI). Tested on a Swiss grid case, the approach reduced SAIDI by over 10% compared to existing methods, demonstrating the effectiveness of directly optimizing reliability metrics. Additionally, the researchers in [1] developed an optimization model structured as a Mixed-Integer Second-Order Cone Program (MISOCP) for service reinstatement in distribution networks with dispersed generation sources, relaxing power flow equations exhibiting non-convexity constraints into a convex conic form. The multi-objective formulation aimed to reduce unserved load and the number of switching actions, and was validated on the IEEE 33-node and Taiwan 84-node networks, demonstrating effective restoration performance. The researchers in [6] developed an optimization model for distribution network restoration, structured as an optimization problem with mixed-integer variables and second-order cone constraints, incorporating network reconfiguration, load rejection, voltage regulation, and DG dispatch while considering load voltage dependency. The proposed model minimized de-energized nodes and self-healing actions, and was validated on a real 83-node distribution system using the Gurobi solver. The researchers in [2] proposed a service restoration model for low-inertia microgrids to address large frequency fluctuations and optimize load restoration. The two-level approach couples a MILP model with a transient simulation to explicitly incorporate system frequency dynamics into the constraints. Validated on a modified IEEE 123-bus system, the results confirm that the proposed model significantly improves the dynamic performance of the system's frequency response during the restoration process.

Similarly, many advanced optimization and modeling techniques have been suggested to cope with the complex challenges of service restoration and resilience in modern distribution networks. The researchers in [16] proposed a bi-level optimization model aimed at enhancing distribution network resilience by integrating islanding strategies with Plug-in Electric Vehicle (PEV) charge/discharge scheduling in electrified parking lots. The upper-level model optimized network islanding to maximize load restoration, while the lower-level model assigned available PEV resources based on proximity and availability. The efficacy of this framework, reformulated as a unilevel optimization model derived through Karush-Kuhn-Tucker optimality conditions, was confirmed via simulations conducted on a standard IEEE 33-node system and a 25-node traffic network, demonstrating improved resilience through coordinated PEV management and driver behavior consideration. The researchers in [17] introduced an approach involving two distinct phases for handling outages in electrical grids. Initially, damaged components were clustered based on proximity to depots and available resources to enhance computational efficiency. The second stage co-optimized repair scheduling, network reconfiguration, and distributed generation dispatch using a mixed-integer linear programming model, and simulations on modified IEEE 34- and 123-bus systems demonstrated that joint optimization of restoration activities significantly improved performance and reduced repair time. In addition, the researchers in [18] analyzed power system robustness occurrences by employing models based on Poisson processes to quantify outage and restoration frequencies, deriving explicit formulas for key resilience metrics such as the performance curve's area, lowest point, and extent. The methodology was demonstrated with empirical data from a common scenario observed in North American transmission systems, providing clearer insights into resilience metric calculations based on restoration rate models. Another

contribution to this problem is study [19], where the researchers proposed a fast service restoration method for medium-voltage distribution systems with distributed generators by integrating intentional islanding and network reconfiguration to maximize load restoration. The approach, which included stages for islanding, connectivity restoration, reconfiguration, and load shedding optimization, was validated on the 69-node system of PG&E, demonstrating its performance. It is also worth noting that the researchers in [20] developed a resilience-oriented restoration method for post-fault operations in secondary distribution networks, addressing challenges such as network protector operation, transformer inrush currents, DG synchronization, and circulating currents. A proactive load recovery framework that segments the outage duration into distinct time intervals was proposed and validated through testing using a customized IEEE 342-bus low-voltage distribution feeder in simulation.

Researchers have introduced innovative optimization frameworks for the strategic deployment of advanced power electronic devices and remotely operable switches to enhance grid resilience and reliability. Moreover, the researchers in [21] introduced an innovative framework for the joint deployment of flexible power electronic devices (SOPs) and remotely operable switches to enhance the robustness of distribution grids, integrating multiple recovery stages and active flexible resource management. The optimization model featuring mixed-integer variables and second-order cone constraints minimized investment and de-energization costs and was validated through simulations evaluated on customized IEEE 34-bus and 123-bus distribution networks. The researchers in [22] proposed mixed-integer convex programming models for the best placement of remote-controlled switches to enhance restoration performance and reliability while controlling costs. The models, aimed at minimizing interruption costs, duration, or maximizing restored loads, were solved efficiently and validated on IEEE 33-bus and 123-bus benchmark feeders, demonstrating effective and timely computation of global optima. In [23], a two-phase, multi-scenario optimization approach is presented for the strategic siting and dimensioning of Soft Open Points. This approach aimed to mitigate power losses and curtailment of distributed generation within distribution networks. The authors employed loss sensitivity and voltage deviation indices for identifying potential SOP locations, while AC power flow-based optimization guided their sizing. Empirical testing on a modified IEEE 33-node system and a 404-node unbalanced network confirmed the method's efficacy.

In summary, studies on multi-criteria optimization of power service recovery within distribution networks have improved grid reliability and efficiency. Mathematical models such as MILP, MISOCP, and robust optimization effectively handle uncertainties in distributed generation and load demands. The integration of advanced devices like Soft Open Points, remote-controlled switches, and Plug-in Electric Vehicle management enhances system resilience. Evolutionary algorithms like SPEA have shown strong performance in solving complex multi-objective problems. Table 1 provides a comparison between this paper and other research, based on the solution methodology, factors considered, and test grids.

Table 1. Comparison between this paper and other work.

Ref.	Solution approach	Multi-objective optimization	Considering the impact of different objective functions	Considering the impact of different load models	Test grid
[1]	MISOCP	YES	YES	NO	33-, 84-node
[6]	MISOCP	YES	NO	NO	Real 83-node
[11]	MIQCP	NO	NO	NO	69-node
[12]	MILP	NO	NO	NO	69-, 246-node
[13]	MILP	NO	NO	NO	123-node
[14]	MILP	NO	NO	NO	13-, 123-node
[15]	MILP	NO	NO	NO	Ewz grid
[16]	MILP	NO	NO	NO	33-node
[17]	MILP	YES	NO	NO	34-, 123-node
[19]	Heuristic	YES	NO	NO	69-node
[20]	Heuristic	YES	NO	NO	342-node
This paper	MISOCP	YES	YES	YES	33-node, Vietnamese 190-node

1.3. Research gaps

Despite extensive research on restoration of power distribution systems, a significant gap remains in the comprehensive and simultaneous analysis of key operational factors. As illustrated in Table 1, while many researchers have explored multi-objective optimization, they often fail to extend this analysis to investigate the profound impact of selecting different objective functions. Furthermore, a notable limitation across the literature is the neglect of different load models when evaluating optimal solutions. To the best of our knowledge, no prior study has presented a comprehensive framework that simultaneously accounts for the use of multi-objective optimization, the impact of various objective functions, and the influence of different load models. This gap highlights the need for a more holistic and realistic approach to power distribution system restoration, which we aim to address.

1.4. Contribution and organization

To overcome these constraints, we introduce a bi-objective MISOCP model for the simultaneous optimization of the total power of unsupplied loads, taking into account the prioritization of demand and the cumulative count of switching actions of sectionalizing devices. This paper's primary contributions are as follows:

- Compared with [11–17, 19, 20], we analyze the impact of different objective functions and varied load models on the optimal solutions.
- Unlike [19, 20], a new MISOCP model that guarantees globally optimal solutions and overcomes the limitations of heuristic and non-linear methods is proposed in this study.
- Unlike [1, 11, 12, 14, 16–20], we utilize a voltage-dependent load model, which accurately reflects the load characteristics in distribution networks. This load model is transformed into the equivalent ZP model by deploying Newton's binomial expansion, enabling efficient solutions using conic solvers.
- Different from [1, 6, 17, 19, 20] with the weight factor method, a heuristic for determining

the Pareto front for the distribution grid restoration problem, where two different objective functions are considered, is used.

- Binary variables are used to incorporate the voltage regulation capability of distributed generating units into the optimization framework.
- Numerical simulations in two test systems: The enhanced IEEE 33-bus and real-world Vietnamese 190-node electrical grids, validating the proposed method's ability to scale and its overall efficacy.
- Novel findings about the 190-bus distribution system are introduced, serving as a crucial benchmark for subsequent research efforts.

The rest of this study is structured into three primary divisions. In Section 2, we propose MINLP and MISOCP models for the multi-objective distribution grid restoration problem, along with introducing a heuristic method to identify the Pareto optimal front for two objective functions. In Section 3, we present the computational results and discussions when the introduced formulation is applied to the adapted 33-bus IEEE benchmark system and a practical 190-node grid. Finally, in Section 4, we conclude this paper with a summary of findings and a discussion of future research directions.

2. Materials and methods

2.1. Problem formulation based on nonlinearly constrained programming with integer variables

The problem of restoring the distribution network after a fault includes objective functions and constraints as described below.

2.1.1. Objective function

The first objective function of the problem of the power distribution system restoration is to minimize the total power of unsupplied loads, taking into account the priority levels of the loads:

$$\min f_1 = \min \sum\nolimits_{i\in\Omega_N} (1-y_i)\left(w_{l1}.P_{l1,i} + w_{l2}.P_{l2,i} + w_{l3}.P_{l3,i}\right) \tag{1}$$

The weighting factors corresponding to load priority groups 1, 2, and 3 are as follows [24]:

$$w_{l1} = \frac{\max P_{l2}}{\min P_{l1}}.\frac{\max P_{l3}}{\min P_{l2}} \tag{2}$$

$$w_{l2} = \frac{\max P_{l3}}{\min P_{l2}} \tag{3}$$

$$w_{l3} = 1 \tag{4}$$

The second objective function of the problem of the distribution network restoration is to minimize the total number of switching operations of sectionalizing devices:

$$\min f_2 = \min\left[\sum_{ij\in\Omega_{ope}} x_{ij} + \sum_{ij\in\Omega_{clo}} \left(1-x_{ij}\right) - \sum_{ij\in\Omega_{ope}} \gamma_{ij}\right] \tag{5}$$

Binary variables γ_{ij} is defined as follows:

$$\gamma_{ij} = 1 - y_i - y_j + x_{ij}, \quad \forall ij \in \Omega_{clo} \tag{6}$$

2.1.2. Constraints of radial topology for distribution systems

The following constraints ensure that the distribution system operates with a radial topology [25]:

$$k_{ij} + k_{ji} = x_{ij}, \quad \forall ij \in \Omega_{\mathrm{L}} \tag{7}$$

$$\sum_{j\in\Omega_{\mathrm{N(i)}}} k_{ij} = y_i, \quad \forall i \in \Omega_{\mathrm{N}}, i \notin \Omega_{sub} \tag{8}$$

$$k_{sub,j} = 0, \quad \forall j \in \Omega_{sub} \tag{9}$$

2.1.3. Model of distributed generation

The voltage regulation capability (PV model) of the DG below represents a universal framework used to investigate DG's voltage control performance during typical operational states. The PV model of the DG is expressed as follows:

$$\beta_i^{\min} + \beta_i^{\max} \le 1;\ \beta_i^{\min} \in \{0;1\};\ \beta_i^{\max} \in \{0;1\};\ \forall i \in \Omega_{\mathrm{DG}} \tag{10}$$

$$U_i^2 \le \left(1-\beta_i^{\min}-\beta_i^{\max}\right)U_{0,i}^2 y_i + \left(\beta_i^{\min}+\beta_i^{\max}\right)\left(U_i^{\max}\right)^2 y_i;\ \forall i \in \Omega_{\mathrm{DG}} \tag{11}$$

$$U_i^2 \ge \left(1-\beta_i^{\min}-\beta_i^{\max}\right)U_{0,i}^2 y_i + \left(\beta_i^{\min}+\beta_i^{\max}\right)\left(U_i^{\min}\right)^2 y_i;\ \forall i \in \Omega_{\mathrm{DG}} \tag{12}$$

$$Q_{\mathrm{DG}i} \le Q_{\mathrm{DG}i}^{\max} + \beta_i^{\min}\left(Q_{\mathrm{DG}i}^{\min} - Q_{\mathrm{DG}i}^{\max}\right);\ \forall i \in \Omega_{\mathrm{DG}} \tag{13}$$

$$Q_{\mathrm{DG}i} \ge Q_{\mathrm{DG}i}^{\min} + \beta_i^{\max}\left(Q_{\mathrm{DG}i}^{\max} - Q_{\mathrm{DG}i}^{\min}\right);\ \forall i \in \Omega_{\mathrm{DG}} \tag{14}$$

$$Q_{\mathrm{DG}i}^{\max} = P_{\mathrm{DG}i}\frac{\sqrt{1-\left(\cos\varphi_{i,lagging}\right)^2}}{\cos\varphi_{i,lagging}};\ Q_{\mathrm{DG}i}^{\min} = -P_{\mathrm{DG}i}\frac{\sqrt{1-\left(\cos\varphi_{i,leading}\right)^2}}{\cos\varphi_{i,leading}};\ \forall i \in \Omega_{\mathrm{DG}} \tag{15}$$

2.1.4. Constraints of power flow equations

Consider a radial power grid consisting of three nodes, *k*, *i*, and *j*, as shown in Figure 1.

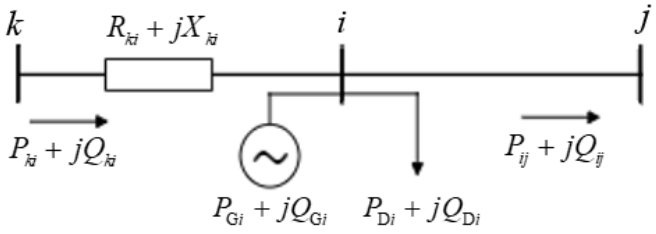

Figure 1. Three-node radial power grid.

The optimization problem involving both mixed-integer variables and nonlinear elements (MINLP), including the equations for steady-state power system operation, is presented as follows:

$$\sum P_{ij} - \left(P_{ki} - R_{ki} \times \frac{P_{ki}^2 + Q_{ki}^2}{U_i^2} \right) = P_{Gi} - P_{Di}; \quad \forall i \in \Omega_N; \forall k, j \in \Omega_{N(i)} \tag{16}$$

$$\sum Q_{ij} - \left(Q_{ki} - X_{ki} \times \frac{P_{ki}^2 + Q_{ki}^2}{U_i^2} \right) = Q_{Gi} - Q_{Di}; \quad \forall i \in \Omega_N; \forall k, j \in \Omega_{N(i)} \tag{17}$$

$$-\left(1 - x_{ij}\right) M \le U_i^2 - U_j^2 - 2\left(R_{ij} P_{ij} + X_{ij} Q_{ij}\right) + \left(R_{ij}^2 + X_{ij}^2\right) \times \frac{P_{ij}^2 + Q_{ij}^2}{U_i^2} \le \left(1 - x_{ij}\right) M; \ \forall ij \in \Omega_L \tag{18}$$

$$-x_{ij} \times M \le P_{ij} \le x_{ij} \times M; \ \forall ij \in \Omega_L \tag{19}$$

$$-x_{ij} \times M \le Q_{ij} \le x_{ij} \times M; \ \forall ij \in \Omega_L \tag{20}$$

2.1.5. Constraints of nodal voltage limits

The voltage magnitude at bus *i* is limited by the maximum value $U_i^{\max}$ and the minimum value $U_i^{\min}$ as follows:

$$y_i \times U_i^{\min} \le U_i \le y_i \times U_i^{\max}; \quad \forall i \in \Omega_N \tag{21}$$

2.1.6. Constraints of branch power flow limits

The power flow on the transmission line *ij* is limited by the maximum value $S_{ij}^{\max}$:

$$P_{ij}^2 + Q_{ij}^2 \le \left(S_{ij}^{\max} \right)^2; \quad \forall ij \in \Omega_L \tag{22}$$

2.1.7. Model of voltage-dependent loads

In the service restoration problem, the real power and reactive power of the load with voltage-responsive characteristics (ZIP load-constant impedance, constant current, constant power) at bus *i* are described as follows:

$$P_{\mathrm{D}i} = y_i \times P_{\mathrm{D}0i}\left(a_i^{\mathrm{P}}U_i^2 + b_i^{\mathrm{P}}U_i + c_i^{\mathrm{P}}\right); \quad i \in \Omega_{\mathrm{D}} \tag{23}$$

$$Q_{\mathrm{D}i} = y_i \times Q_{\mathrm{D}0i}\left(a_i^{\mathrm{Q}}U_i^2 + b_i^{\mathrm{Q}}U_i + c_i^{\mathrm{Q}}\right); \quad i \in \Omega_{\mathrm{D}} \tag{24}$$

$$a_i^{\mathrm{P}} + b_i^{\mathrm{P}} + c_i^{\mathrm{P}} = 1; \quad a_i^{\mathrm{Q}} + b_i^{\mathrm{Q}} + c_i^{\mathrm{Q}} = 1; \tag{25}$$

If bus *i* is not energized, i.e., $y_i = 0$, then the active and reactive powers of the load are both zero. If bus *i* is energized, i.e., $y_i = 1$, then the active and reactive powers of the load are determined by expressions similar to those in [3].

2.2. Linearization of nonlinear components

2.2.1. Second-order cone model of power flow equations

The nonlinear components of Eqs (16–20) are the squared current magnitude $\left(\frac{P_{ki}^2 + Q_{ki}^2}{U_i^2}\right)$ flowing through the distribution line and the square of the voltage magnitude at node *i* $\left(U_i^2\right)$.

Let $I_{ki} = \frac{P_{ki}^2 + Q_{ki}^2}{U_i^2}$ and $V_i = U_i^2$, and the constraints (16–20) are transformed as follows:

$$\sum P_{ij} - \left(P_{ki} - R_{ki} \times I_{ki}\right) = P_{\mathrm{G}i} - P_{\mathrm{D}i}; \ \forall i \in \Omega_{\mathrm{N}}, \forall k, j \in \Omega_{\mathrm{N(i)}} \tag{26}$$

$$\sum Q_{ij} - \left(Q_{ki} - X_{ki} \times I_{ki}\right) = Q_{\mathrm{G}i} - Q_{\mathrm{D}i}; \ \forall i \in \Omega_{\mathrm{N}}, \forall k, j \in \Omega_{\mathrm{N(i)}} \tag{27}$$

$$-\left(1 - x_{ij}\right)M \le V_i - V_j + \left(R_{ij}^2 + X_{ij}^2\right) \times I_{ij} - 2\left(R_{ij}P_{ij} + X_{ij}Q_{ij}\right) \le \left(1 - x_{ij}\right)M; \quad \forall ij \in \Omega_{\mathrm{L}} \tag{28}$$

$$-x_{ij} \times M \le P_{ij} \le x_{ij} \times M; \ -x_{ij} \times M \le Q_{ij} \le x_{ij} \times M; \quad \forall ij \in \Omega_{\mathrm{L}} \tag{29}$$

The constraint (21) is transformed as follows:

$$y_i \times \left(U_i^{\min}\right)^2 \le V_i \le y_i \times \left(U_i^{\max}\right)^2; \quad \forall i \in \Omega_{\mathrm{N}} \tag{30}$$

The following expression represents the second-order cone constraint:

$$P_{ij}^2 + Q_{ij}^2 \le I_{ij}V_i; \quad \forall ij \in \Omega_{\mathrm{L}} \tag{31}$$

2.2.2. Equivalent ZP model of voltage-dependent loads

Under normal operating conditions, the voltage magnitudes at all buses are approximately 1 p.u., so applying Newton's binomial expansion gives the following expressions:

$$U_i^{\eta} = (1+\Delta U_i)^{\eta} \approx 1+\eta\Delta U_i; \quad i=1,...,N \tag{32}$$

where, U_i is the voltage magnitude at node *i*, and η is a constant such that $|\eta\Delta U_i| << 1$.

With $\eta = 2$ and $U_i = 1+\Delta U_i$, so Eq (33) is achieved:

$$V_i = U_i^2 = (1+\Delta U_i)^2 = 1+2\Delta U_i; \quad i=1,...,N \tag{33}$$

The ZIP load model (23) can be approximated by an equivalent ZP model, with coefficients derived from the original ZIP load model. From Eqs (23) and (33), the following expression is achieved:

$$\begin{aligned} P_{\mathrm{D}i} &= y_i \times P_{\mathrm{D}0i}\left[c_i^{\mathrm{P}} + a_i^{\mathrm{P}}U_i^2 + b_i^{\mathrm{P}}(1+\Delta U_i)\right] \\ &\approx y_i \times P_{\mathrm{D}0i}\left[\left(c_i^{\mathrm{P}} + \frac{b_i^{P}}{2}\right) + \left(a_i^{\mathrm{P}} + \frac{b_i^{P}}{2}\right)V_i\right]; \quad \forall i \in \Omega_{\mathrm{D}} \end{aligned} \tag{34}$$

Similarly, the reactive power of the equivalent ZP model is given by:

$$Q_{\mathrm{D}i} = y_i \times Q_{\mathrm{D}0i}\left[\left(c_i^{\mathrm{Q}} + \frac{b_i^{Q}}{2}\right) + \left(a_i^{\mathrm{Q}} + \frac{b_i^{Q}}{2}\right)V_i\right]; \ \forall i \in \Omega_{\mathrm{D}} \tag{35}$$

When $y_i = 0$, the load power for both the original ZIP and the equivalent ZP models is zero. When $y_i = 1$, the error of the equivalent ZP model compared to the original ZIP model for commercial loads is presented in Table 2. The coefficients of the ZIP load model are referenced from [3], and the values of $P_{\mathrm{D}0}$ and $Q_{\mathrm{D}0}$ are taken as 1.0 per unit. The voltage variation range in steady-state mode is set to [0.9, 1.1]. Table 2 shows that the largest errors in active and reactive powers between the two models are 0.448% and 2.244%, respectively. A similar analysis shows that the largest errors in active and reactive powers for residential and industrial loads are both lower than those for commercial loads. Therefore, the equivalent ZP model has a very small error compared to the original ZIP model.

Constraints (34) and (35) contain nonlinear terms that include a term formed by multiplying a binary variable and a continuous variable. The exact linearization technique for such a product is described as follows:

$$\begin{aligned} P_{\mathrm{D}i} &= y_i \times P_{\mathrm{D}0i} \times \left(c_i^{\mathrm{P}} + \frac{b_i^{\mathrm{P}}}{2}\right) + P_{\mathrm{D}0i} \times \left(a_i^{\mathrm{P}} + \frac{b_i^{\mathrm{P}}}{2}\right)V_i \times y_i; \quad \forall i \in \Omega_{\mathrm{D}} \\ Q_{\mathrm{D}i} &= y_i \times Q_{\mathrm{D}0i} \times \left(c_i^{\mathrm{Q}} + \frac{b_i^{Q}}{2}\right) + Q_{\mathrm{D}0i} \times \left(a_i^{\mathrm{Q}} + \frac{b_i^{\mathrm{Q}}}{2}\right)V_i \times y_i; \quad \forall i \in \Omega_{\mathrm{D}} \end{aligned} \tag{36}$$

Let

$$V_{l,i} = V_i.y_i; \quad \forall i \in \Omega_{\mathrm{D}} \tag{37}$$

$$V_{l,i} = \begin{cases} 0 & \text{if} \quad y_i = 0 \\ V_i & \text{if} \quad y_i = 1 \end{cases} \tag{38}$$

Using the linearization method for the multiplicative term involving a binary variable and a continuous variable, the expression (36) is transformed into the following linear form:

$$\begin{aligned} P_{\mathrm{D}i} &= y_i \times P_{\mathrm{D}0i} \times \left(c_i^{\mathrm{P}} + \frac{b_i^{\mathrm{P}}}{2} \right) + P_{\mathrm{D}0i} \times \left(a_i^{\mathrm{P}} + \frac{b_i^{\mathrm{P}}}{2} \right) V_{l,i}; \quad \forall i \in \Omega_{\mathrm{D}} \\ Q_{\mathrm{D}i} &= y_i \times Q_{\mathrm{D}0i} \times \left(c_i^{\mathrm{Q}} + \frac{b_i^{Q}}{2} \right) + Q_{\mathrm{D}0i} \times \left(a_i^{\mathrm{Q}} + \frac{b_i^{\mathrm{Q}}}{2} \right) V_{l,i}; \quad \forall i \in \Omega_{\mathrm{D}} \end{aligned} \tag{39}$$

The constraint (37) is linearized as follows:

$$V_{l,i} = V_i - d_i; \quad \forall i \in \Omega_{\mathrm{D}} \tag{40}$$

$$-M \times y_i \le V_{l,i} \le M \times y_i; \quad \forall i \in \Omega_{\mathrm{D}} \tag{41}$$

$$-M \times (1 - y_i) \le d_i \le M \times (1 - y_i); \quad \forall i \in \Omega_{\mathrm{D}} \tag{42}$$

When the node *i* is energized $(y_i = 1)$, constraints (40–42) force $d_i = 0$ and $V_{l,i} = V_i$. When the node *i* is de-energized $(y_i = 0)$, constraints (40–42) force $V_{l,i} = 0$ and $V_i = d_i$.

Table 2. Comparison between two load models for commercial loads.

Voltage (p.u.)	Original ZIP model		Equivalent ZP model		Error	
	$P_{\mathrm{D}}(\mathrm{p.u.})$	$Q_{\mathrm{D}}(\mathrm{p.u.})$	$P_{\mathrm{D}}(\mathrm{p.u.})$	$Q_{\mathrm{D}}(\mathrm{p.u.})$	$P_{\mathrm{D}}(\%)$	$Q_{\mathrm{D}}(\%)$
0.90	0.8896	0.6906	0.8936	0.6751	0.448	2.244
0.91	0.9005	0.7186	0.9037	0.7061	0.359	1.747
0.92	0.9114	0.7473	0.9140	0.7373	0.280	1.328
0.93	0.9224	0.7766	0.9243	0.7690	0.212	0.978
0.94	0.9334	0.8065	0.9348	0.8010	0.154	0.692
0.95	0.9444	0.8372	0.9454	0.8333	0.106	0.463
0.96	0.9555	0.8684	0.9561	0.8659	0.067	0.286
0.97	0.9665	0.9003	0.9669	0.8989	0.037	0.155
0.98	0.9777	0.9329	0.9778	0.9323	0.016	0.066
0.99	0.9888	0.9661	0.9889	0.9660	0.004	0.016
1.00	1.0000	1.0000	1.0000	1.0000	0.000	0.000
1.01	1.0112	1.0345	1.0113	1.0344	0.004	0.015

Continued on next page

Voltage (p.u.)	Original ZIP model		Equivalent ZP model		Error	
	$P_{\mathrm{D}}(\mathrm{p.u.})$	$Q_{\mathrm{D}}(\mathrm{p.u.})$	$P_{\mathrm{D}}(\mathrm{p.u.})$	$Q_{\mathrm{D}}(\mathrm{p.u.})$	$P_{\mathrm{D}}(\%)$	$Q_{\mathrm{D}}(\%)$
1.02	1.0225	1.0697	1.0226	1.0691	0.016	0.058
1.03	1.0337	1.1055	1.0341	1.1041	0.035	0.126
1.04	1.0451	1.1420	1.0457	1.1395	0.061	0.217
1.05	1.0564	1.1792	1.0574	1.1753	0.095	0.329
1.06	1.0678	1.2169	1.0692	1.2114	0.135	0.459
1.07	1.0792	1.2554	1.0811	1.2478	0.181	0.605
1.08	1.0906	1.2945	1.0932	1.2845	0.234	0.766
1.09	1.1021	1.3342	1.1053	1.3217	0.293	0.941
1.10	1.1136	1.3746	1.1176	1.3591	0.358	1.128

2.3. Problem formulation based on conic quadratic programming with integer variables

The MISOCP model is formulated, including: Objective functions (1) and (5); radial network structure constraints (7–9); distributed generation model constraints (10–15); branch power flow limit constraints (22); the mathematical models characterizing the power system's performance under steady-state conditions (26–31); and voltage-dependent load power constraints (39–42).

2.4. Multi-objective optimization with Pareto front

The proposed MISOCP model can be addressed through an optimization problem with multiple objectives, where the total unserved load power-considering load priority and the cumulative count of sectionalizing device switching actions are treated as two separate objective functions. These two objectives are conflicting: Minimizing the total non-restored load power requires performing more switching operations on sectionalizing devices, whereas reducing the total count of switching actions tends to increase the total non-restored load power. The optimization problem involving multiple objectives based on the proposed MISOCP model, aimed at solving the post-fault distribution network restoration problem, is presented mathematically in Eq (43):

$$\min\left\{f_1(x), f_2(x)\right\} \tag{43}$$

where f_1 represents the total non-restored load power considering load priority, f_2 is the overall count of sectionalizing device switching actions, and x denotes the grid configuration after restoration. Multi-objective optimization enables obtaining a collection of Pareto optimal outcomes, often referred to as the Pareto optimal frontier. An outcome x is considered Pareto optimal if no other solution exists that is superior in all objectives, meaning that there exists no other outcome x' that simultaneously fulfills $f_1(x) > f_1(x')$ and $f_2(x) > f_2(x')$.

To derive the Pareto optimal frontier for the multi-objective optimization problem, a restriction on the total number of sectionalizing device switching operations is added to the model, as given in (44):

$$f_2 = \sum_{ij\in\Omega ope} x_{ij} + \sum_{ij\in\Omega clo}\left(1-x_{ij}\right) - \sum_{ij\in\Omega ope}\gamma_{ij} < \overline{f}_2^{(k)} \tag{44}$$

Each solution k on the Pareto front is identified by setting an appropriate upper bound on the count of switching actions $\left(\overline{f}_2^{(k)}\right)$ and solving the respective optimization problem as follows:

$$\begin{aligned} &\min f_1 \\ &\text{subject to} \\ &\quad \text{constraints}\,(7)-(9),(10)-(15),(22),(26)-(31) \\ &\quad (39)-(42), \text{and}\,(44) \end{aligned} \tag{45}$$

The first resolution is found by setting the switching operation boundary to a very high value. The ensuing resolution is determined by setting the switching operation boundary equal to the number of switching operations of the solution obtained previously. The procedure is iteratively executed until the problem's feasibility is no longer maintained.

Moreover, the fuzzy set theory is applied as an effective method to analyze and identify Pareto resolutions within the realm of multi-criteria optimization [8]. After obtaining the set of Pareto best solutions, the introduced method employs a mechanism employing the fuzzy set theory to select a balanced Pareto optimal resolution, ensuring a trade-off between conflicting criteria. This solution is referred to as the balanced Pareto optimal solution. The value of the μ_n objective function for each solution in the Pareto optimal set is represented by a membership function defined as follows:

$$\mu_n = \begin{cases} 1 & , \quad F_n \le F_n^{\min} \\ \dfrac{F_n^{\max} - F_n}{F_n^{\max} - F_n^{\min}}, & F_n^{\min} < F_n < F_n^{\max} \\ 0 & , \quad F_n \ge F_n^{\max} \end{cases} \tag{46}$$

where F_n is the best outcome of the objective function n; $F_n^{\min}$ and $F_n^{\max}$ are the minimum and maximum of the objective function's values, n, respectively.

For each Pareto optimal solution k in the solution set, the membership function $\mu^{(k)}$, representing that solution, is defined by the equation below:

$$\mu^{(k)} = \frac{\sum_{n=1}^{N} \mu_n^{(k)}}{\sum_{m=1}^{M} \sum_{n=1}^{N} \mu_n^{(m)}} \tag{47}$$

where N is the number of objective functions in the problem, and M is the number of Pareto optimal solutions in the solution set.

The balanced Pareto optimal solution is the highest one with the membership function $\mu^{(k)}$ value among the set of optimal solutions of the problem.

2.5. Recovery strategy and flowchart of optimization algorithm

When a permanent fault occurs in a distribution network, protection devices act immediately to clear the fault current. Affected distributed generating units are simultaneously disconnected by anti-islanding protection. Furthermore, the supervisory control and data acquisition (SCADA) system collects crucial system data, which a self-healing system then processes to conduct fault location and develop a restoration strategy that considers the contributions of DGs. This information is then used by the execution unit to first isolate the fault, execute the restoration strategy, and then reconnect the DGs to the network. Maintenance crews are subsequently dispatched to repair the faulted elements. Given that service restoration is an emergency procedure, it has two major objectives: To restore as much service as possible to affected customers and to perform the process as quickly as possible to minimize the blackout area [1].

Network reconfiguration serves as the foundation for the restoration strategies in this study. This process must satisfy several operational constraints, such as power balance, nodal voltages, branch ratings, and a radial topology.

To illustrate the service restoration procedure, we use the test system shown in Figure 2(a). When a fault occurs on branch 2–9, the switch on this branch opens to isolate the fault, leaving the loads at nodes 9–12 de-energized. An optimization model then develops a restoration scheme. After executing the scheme, the switch on branch 8–11 is closed, re-energizing the loads in the fault area. The final post-restoration topology of the system is shown in Figure 2(b).

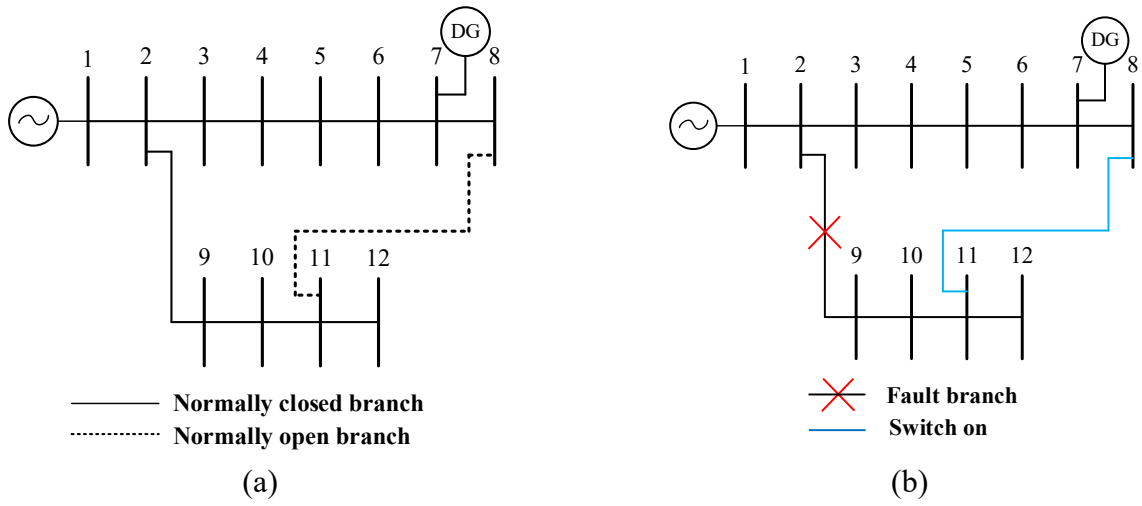

Figure 2. Illustration of restoration strategy based on network reconfiguration.

Figure 3 illustrates the flowchart of the optimization algorithm, which is designed to assess the impact of different objective functions and various load models. This flowchart serves as a roadmap for understanding the logical steps of our methodology.

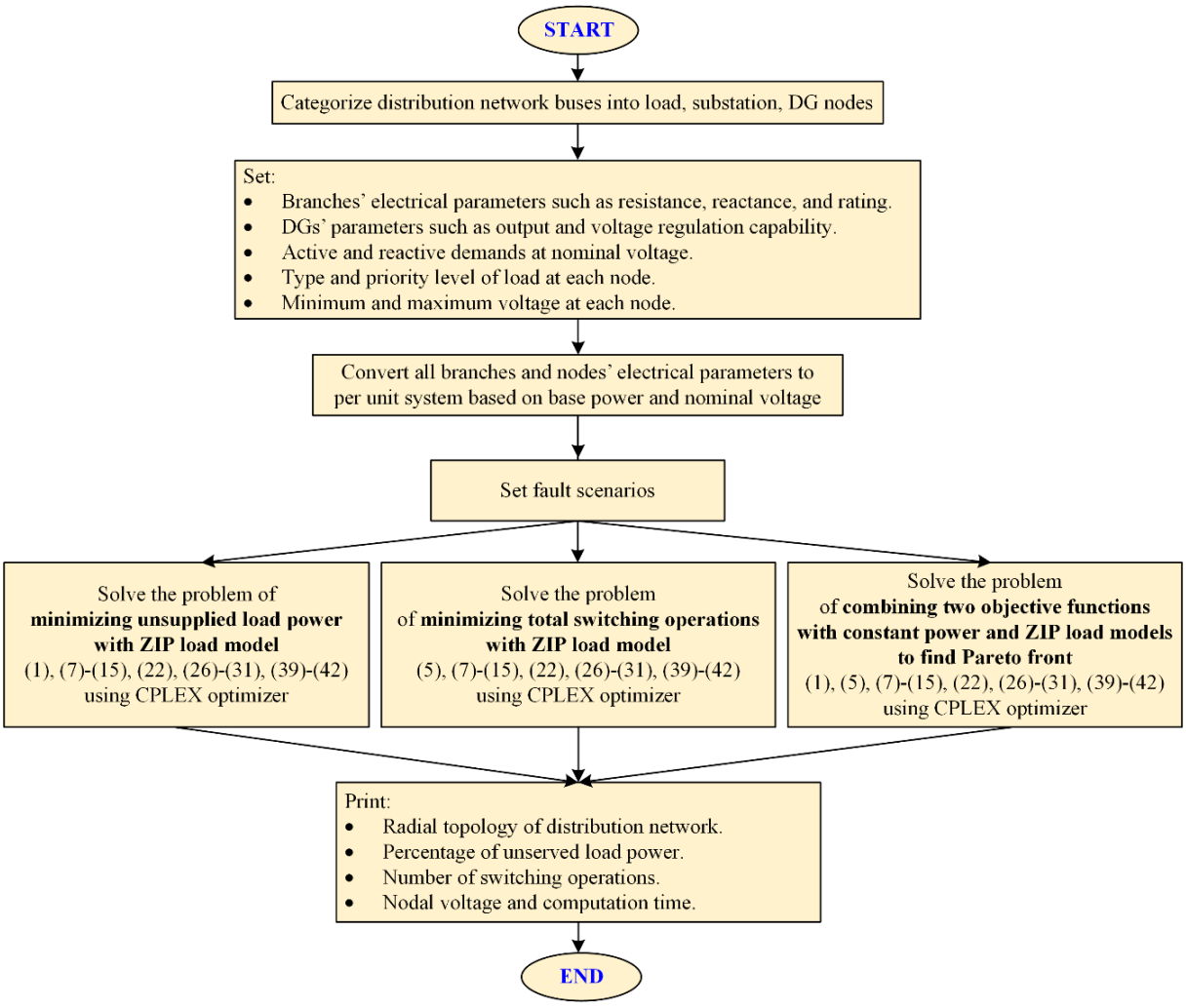

Figure 3. Flowchart of the optimization algorithm for the proposed service restoration.

3. Results

In this study, the MISOCP model is put into practice to optimally restore the modified IEEE 33-node distribution network and the Vietnamese 190-bus distribution system, taking into account voltage-sensitive load behavior and the involvement of distributed energy resources following fault conditions. We use the CPLEX solver along with the GAMS programming language [26] to determine optimal solutions. All computational results presented in this paper are obtained on a personal computer equipped with an Intel Core i7-13620H processor and 32 GB of RAM. To guarantee the quality of the solution, the optimality gap, which serves as the mixed-integer solver's termination criterion, is set to 0% in all simulations.

Figure 4 outlines the computational scenarios for the proposed service restoration model, which account for the influence of different objective functions and distinct load models.

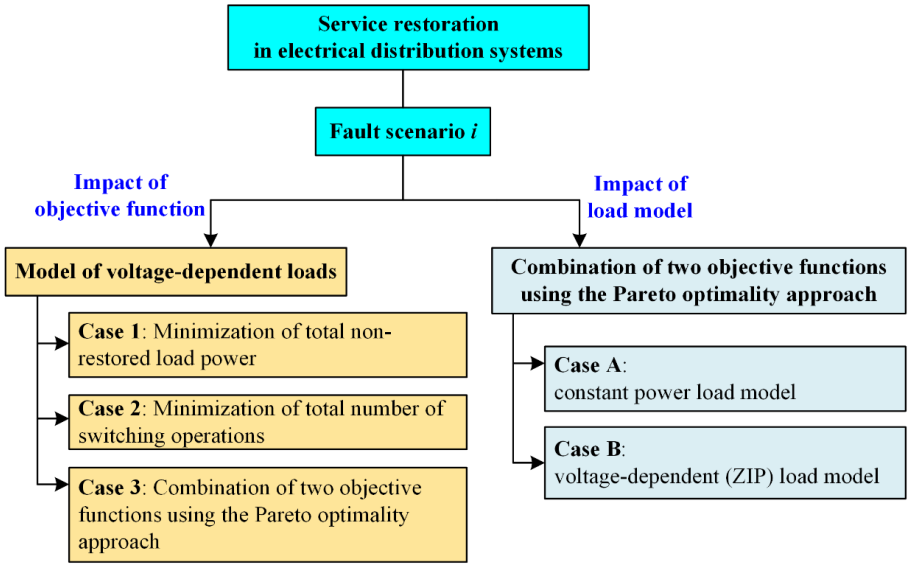

Figure 4. Summary of considered scenarios.

3.1. Modified IEEE 33-node test system

3.1.1. Data description

The modified IEEE 33-bus distribution system [27] is illustrated in Figure 5. For enhanced efficiency and rapid response during power outages, every individual branch within the distribution network is outfitted with a remote-control switch, enabling automated operations as an integral part of the service restoration process, thus significantly reducing manual intervention and downtime. Four DG units are installed at nodes 7, 10, 14, and 33. Details concerning the distributed generation units can be found in Table 3. Additionally, the operating voltage is set at 1.0 per unit when the DGs are modeled as PV-type sources. The necessary parameters for distribution network calculations are presented concisely in Table 4.

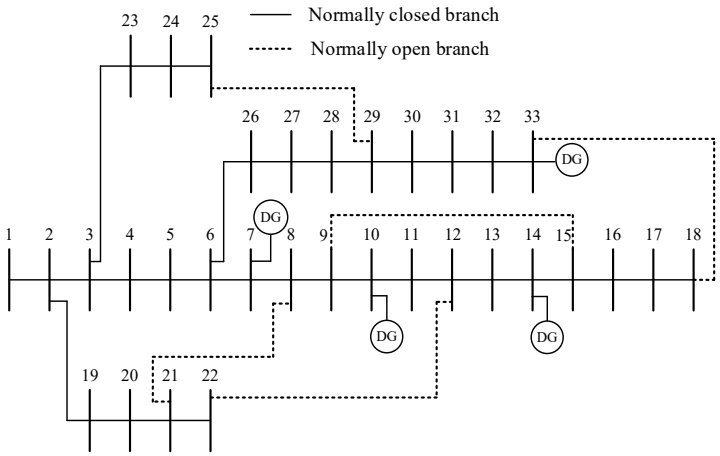

Figure 5. Modified IEEE 33-node distribution network.

Table 3. Distributed generation data.

Location	P_{DG} (kW)	PV model	
		$\cos\varphi_{DG,leading}$	$\cos\varphi_{DG,lagging}$
7	350	0.95	0.95
10	400		
14	450		
33	500		

Table 4. The dataset for the adapted IEEE 33-bus distribution system.

Parameter	Value
Nominal voltage (kV)	12.66
Total load power (kVA)	$3715 + j2300$
Allowable voltage limits at the nodes (p.u.)	$0.9 \le U \le 1.1$
Maximum transferable power on each branch (MVA)	10
Base power (MVA)	10
Base voltage (kV)	12.66

The three types of loads considered in this section are residential, commercial, and industrial loads. The load type corresponding to each node is presented in Table 5. The coefficients of the ZIP load representation corresponding to each load type in the per-unit system are given as follows [3].

- Residential: $a_i^{\mathrm{P}} = 0.24; b_i^{\mathrm{P}} = 0.62; c_i^{\mathrm{P}} = 0.13; a_i^{\mathrm{Q}} = 2.44; b_i^{\mathrm{Q}} = -1.94; c_i^{\mathrm{Q}} = 0.50;$
- Commercial: $a_i^{\mathrm{P}} = 0.16; b_i^{\mathrm{P}} = 0.80; c_i^{\mathrm{P}} = 0.04; a_i^{\mathrm{Q}} = 3.26; b_i^{\mathrm{Q}} = -3.10; c_i^{\mathrm{Q}} = 0.84;$
- Industrial: $a_i^{\mathrm{P}} = -0.07; b_i^{\mathrm{P}} = 0.24; c_i^{\mathrm{P}} = 0.83; a_i^{\mathrm{Q}} = 1.00; b_i^{\mathrm{Q}} = 0; c_i^{\mathrm{Q}} = 0.$

Table 5. Load characteristics of the IEEE 33-node network.

Load	Node
Residential	2, 5, 12, 14, 19, 22, 31, 32
Commercial	4, 7, 8, 10, 11, 13, 15, 17, 20, 23, 24, 25, 26, 28, 29, 30, 33
Industrial	3, 6, 9, 16, 18, 21, 27

Table 6 provides information on the priority levels of the loads.

Table 6. Load priority levels of the IEEE 33-node network.

Priority Levels	Node
1	1–3, 9–11, 14, 32, 33
2	4, 5, 12, 15, 18–21, 25, 26, 29
3	6–8, 13, 17, 22–24, 27, 28, 30, 31

The optimal distribution network restoration model after faults is calculated and compared on the IEEE 33-bus system under three fault location scenarios on the network, specifically:

- Scenario 1: Fault on the line branch 2–3.
- Scenario 2: Fault on the line branch 2–19.
- Scenario 3: Faults on the line branches 4–5 and 13–14.
- Scenario 4: Fault at node 5.

3.1.2. Impact of the objective function

Here, we investigate the effects of diverse objective functions on the optimal structure of the distribution network after a fault, considering three objective functions, including:

- Objective function f_1: Minimization of the total non-restored load power considering load priority;
- Objective function f_2: Minimization of the cumulative count of sectionalizing switch actuations;
- Objective functions f_1 and f_2: A combination of both objectives using the Pareto optimal solution approach.

The PV model of the distributed generation sources is considered. The ZIP load model is applied for calculations. After computations using the GAMS programming software, the Pareto optimal solutions $(p;s)$ of the fault scenarios with the combined objective functions $\{f_1, f_2\}$ are presented in Table 7, where p is the percentage of load power not restored; and s represents the cumulative count of sectionalizing device switching operations. The collection of Pareto-efficient outcomes (also called the Pareto front) for fault scenario 2 is illustrated in Figure 6.

Table 7. The set of Pareto-efficient outcomes for the IEEE 33-node system.

Fault scenario	Pareto optimal solution $(p;s)$
1	(0.96%; 7), (4.9%; 5), (5.24%; 2)
2	(0.98%; 7), (2.01%; 6), (2.62%; 5), (3.63%; 3), (5.24%; 2), (7.68%; 1)
3	(0%; 8), (0.54%; 5), (1.31%; 3)
4	(0.71%; 9), (1.3%; 4), (2.23%; 2)

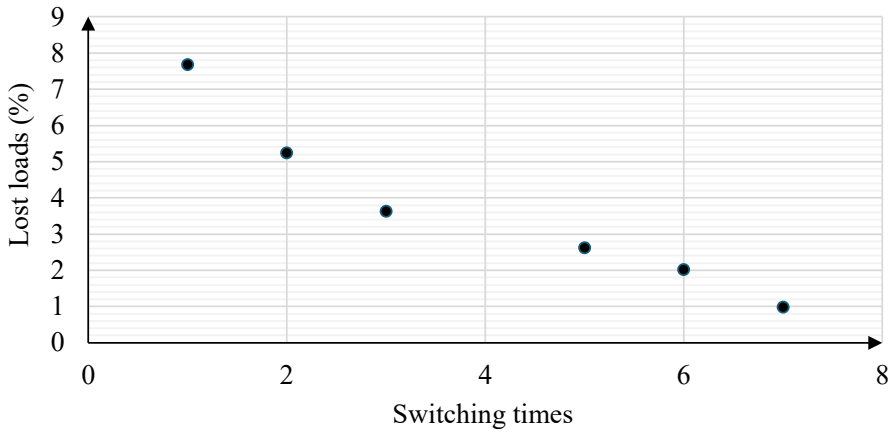

Figure 6. Pareto front of the fault Scenario 2 for the IEEE 33-node system.

According to the formulas described in Eqs (46) and (47), the balanced Pareto optimal solutions are identified as follows: For the fault at branch 2–3, the lost load power is 0.96%, corresponding to 7 switching operations; for the fault at branch 2–19, the lost load power is 3.63%, corresponding to 3 switching operations; and for the simultaneous faults at branches 4–5 and 13–14, the lost load power is 0.54%, corresponding to 5 switching operations.

The optimal results of the problem with individual objective functions f_1, f_2, and the combined objective function $\{f_1, f_2\}$ (corresponding to the balanced Pareto optimal solution) for the fault scenarios are shown in Table 8.

Table 8. Impact of objective functions on the IEEE 33-node network.

Scenario	Objective function	The status of the sectionalizing devices changed after the fault		Number of sectionalizing device switching operations	Total percentage of load power not restored (%)
		Closed sectionalizing device	Open sectionalizing device		
1	f_1	9–15; 12–22; 18–31; 25–29	11–12; 23–24; 24–25; 29–30; 30–31	9	0.96
	f_2	8–21	5–6	2	16.54
	$\{f_1, f_2\}$	12–22; 18–33; 25–29	23–24; 24–25; 29–30; 30–31	7	0.96
2	f_1	9–15; 12–22; 18–31; 25–29	3–23; 11–12; 24–25; 26–27; 28–29	9	0.98
	f_2	/	24–25	1	7.68
	$\{f_1, f_2\}$	18–33	29–30; 31–32	3	3.63
3	f_1	8–21; 9–15; 12–22; 18–31; 25–29	9–10; 24–25; 28–29	8	0
	f_2	9–15; 12–22	2–3	3	15.88
	$\{f_1, f_2\}$	9–15; 18–33; 25–29	29–30; 31–32	5	0.54
4	f_1	8–21; 9–15; 12–22; 18–33; 25–29	8–9; 13–14; 24–25; 28–29	9	0.71
	f_2	12–22	3–4	2	2.23
	$\{f_1, f_2\}$	18–33; 25–29	29–30; 31–32	4	1.3

The findings in Table 8 suggest that:

- For Scenario 1, when optimizing according to the objective function f_1, the fraction of unmet demand is 0.96%, but requires 9 switching operations. Conversely, when optimizing according to the objective function f_2, only 2 switching operations are needed, but the load not restored increases to 16.54%. When combining both objectives $\{f_1, f_2\}$, the results are more balanced with 0.96% load not restored and 7 switching operations.
- For Scenario 2, when optimizing according to the objective function f_1, the fraction of unmet demand is only 0.98% with 9 switching operations, whereas optimizing according to the

objective function f_2 requires only 1 switching operation, but the load not restored is 7.68%. The combined objective function $\{f_1, f_2\}$ results in a 3.63% load not being restored with 3 switching operations.

- For Scenario 3, when optimizing according to the objective function f_1, all loads are restored with 8 switching operations, while optimizing according to the objective function f_2 requires only 3 switching operations, but the unrecovered load ratio remains high (15.88%). When combining both objectives $\{f_1, f_2\}$, the load not restored rate is very low at 0.54% with 5 switching operations.
- For Scenario 4, when optimizing to minimize unserved load f_1, the unserved load percentage is only 0.71% with 9 switching operations. In contrast, optimizing to minimize switching operations f_2 requires 2 switching operations, but the unserved load is 2.23%. The combined objective function $\{f_1, f_2\}$ helps reduce the unserved load percentage to 1.3% with 4 switching operations.

Thus, the combined objective function based on the Pareto optimality principle demonstrates the ability to generate highly balanced and flexible operational plans, which is particularly useful for decision-making support.

3.1.3. Impact of load model

Here, we investigate the influence of the load modeling approach on the optimal network topology following a fault. The optimization model simultaneously employs two objective functions $\{f_1, f_2\}$. Consideration is given to two different load models: The fixed-power load model (constant P load) and the voltage-dependent load model (ZIP load). DG is modeled using the PV bus model and is included in the calculations. The optimal solution of the problem, corresponding to the balanced Pareto optimal solution determined according to Eqs (46) and (47), is presented in Table 9.

The calculation results from Table 9 show a clear distinction between load models in determining the optimal operating structure of the distribution system after a fault, the total count of switching actions on sectionalizing devices, and the total amount of unserved load. In Scenario 1, the unserved load percentage decreases from 5.52% (constant power load model) to 0.96% (ZIP load model), while the total count of switching actions increases from 3 to 7, respectively. In contrast, in Scenario 2, the unserved load percentage with the constant power load model (1.34%) is lower than with the ZIP load model (3.63%), and the number of switching operations decreases from 7 to 3 accordingly. In Scenario 3, the unserved load percentage decreases from 5.47% (constant power load) to 0.54% (ZIP load), but the number of switching operations increases from 4 to 5. Furthermore, in Scenario 4, the unserved load percentage decreases from 5.05% (constant power load) to 1.3% (ZIP load), but the corresponding number of switching operations increases from 4 to 5.

The differences in Table 9 primarily stem from the distinct mechanisms of the constant power load model versus the voltage-dependent load model. With the constant power model, the load always demands power equal to its nominal value. If the grid voltage drops, the load draws a larger current to maintain that power level, which in turn causes more severe voltage drops on the lines. To avoid these severe drops and keep nodal voltages within permissible limits, the algorithm may be forced to restore only a portion of the load. Conversely, with the ZIP load model, power consumption decreases as the

voltage drops, which helps improve the voltage profile. This gives the optimization model more flexibility to find a feasible solution that restores a larger amount of load.

The comparison of these models not only highlights the necessity of selecting an appropriate load model but also underscores the importance of incorporating realistic load characteristics into the optimization problem. This is particularly essential in emergency operations or when facing complex contingencies, where decisions based on accurate modeling directly impact the efficiency and reliability of the power system. The optimal network configurations for Scenario 2, corresponding to the fixed-power load representation and the ZIP-type load model, are illustrated in Figure 7, respectively.

Additionally, the voltage profile of the distribution network under the three fault scenarios, when applying two load models, the fixed-power load model (constant power load) and the voltage-dependent load framework (ZIP load), is presented in Figure 8. The calculation results from the graphs indicate that changing the load framework affects the bus voltage profile across the scenarios.

- In Scenario 1, the constant power load model has a lowest voltage of 0.9475 per unit (at bus 30) and 4 buses (22–25) with load not restored. In contrast, the ZIP load model has a minimum voltage of 0.9282 p.u. (at bus 25) but only 2 buses (24, 30) with loads not restored.
- In Scenario 2, the minimum voltages are 0.9725 p.u. (constant power load) and 0.9826 p.u. (ZIP load) at the same bus 25. However, the total number of buses with load not restored is 4 (buses 23, 24, 30–31) for the fixed-power load model and 6 (buses 19–22, 30–31) for the ZIP-type load representation.
- In Scenario 3, the difference is more pronounced, with the ZIP load model having a lowest voltage of 0.9858 per unit (at bus 25), which is significantly higher than 0.9412 p.u. (at bus 30) under the fixed-power load framework. Moreover, the number of buses without power supply decreases from 4 buses (13, 23–25) under the constant power load model to only 2 buses (30, 31) under the ZIP load model.

Table 9. Impact of load model on the network configuration of the IEEE 33-node grid.

Scenario	Load Model	Status of Sectionalizing Devices Changed After the Fault		Number of sectionalizing device switching operations	Total percentage of load power not restored (%)
		Closed Sectionalizing Devices	Open Sectionalizing Device		
1	Constant Power Load	8–21	3–23; 21–22	3	5.52
	ZIP Load	12–22; 18–33; 25–29	23–24; 24–25; 29–30; 30–31;	7	0.96
2	Constant Power Load	12–22; 18–33; 25–29	3–23; 24–25; 29–30; 31–32	7	1.34
	ZIP Load	18–33	29–30; 31–32	3	3.63
3	Constant Power Load	8–21; 18–33	3–23; 12–13	4	5.47
	ZIP Load	9–15; 18–33; 25–29	29–30; 31–32	5	0.54
4	Constant Power Load	8–21; 18–33	3–4; 6–26; 31–32	5	5.05
	ZIP Load	18–33; 25–29	29–30; 31–32	4	1.3

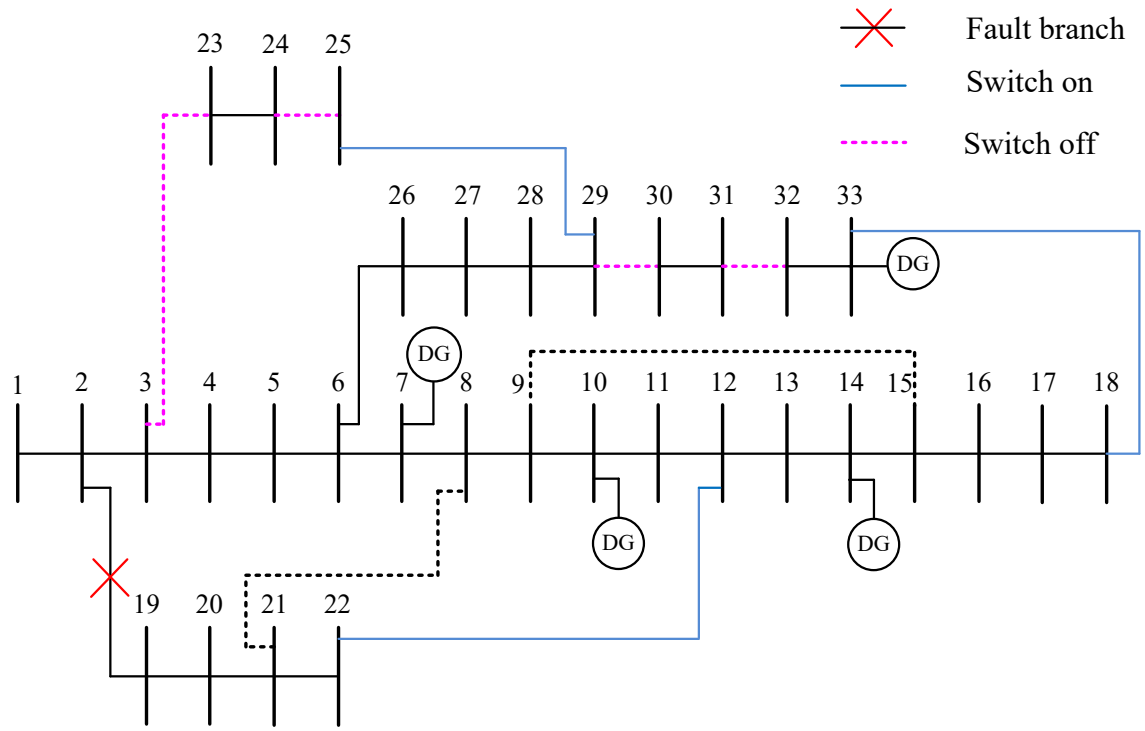

(a) Constant power load.

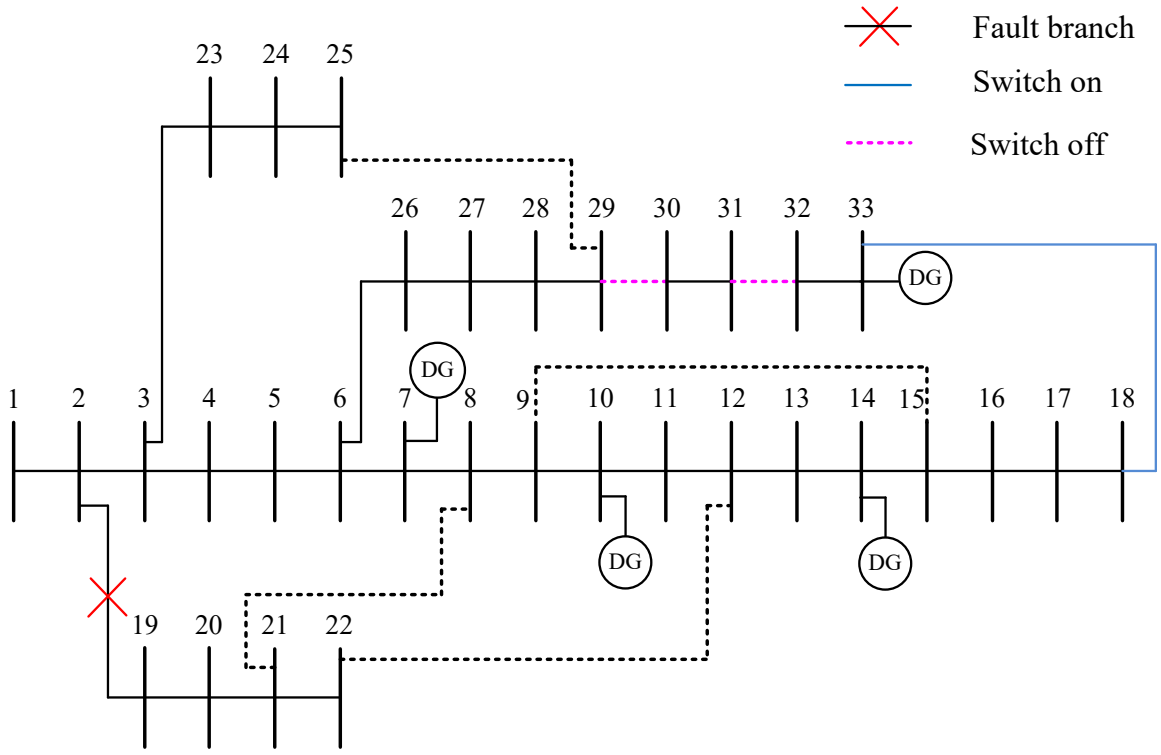

(b) ZIP load.

Figure 7. Network configuration in Scenario 2 considering the impact of different load models.

(a) Scenario 1.

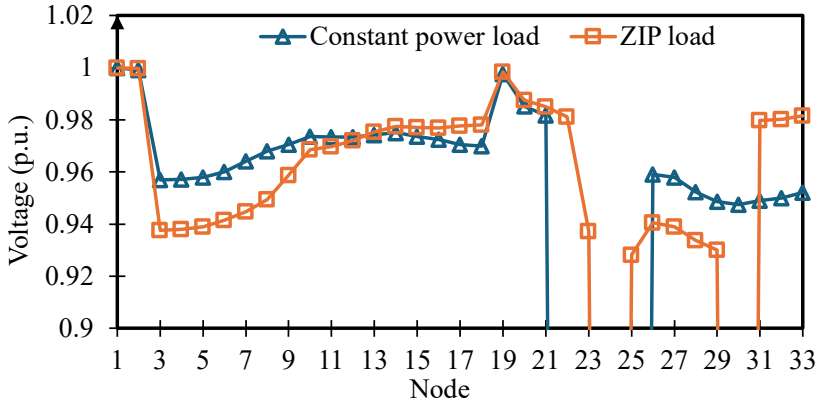

(b) Scenario 2.

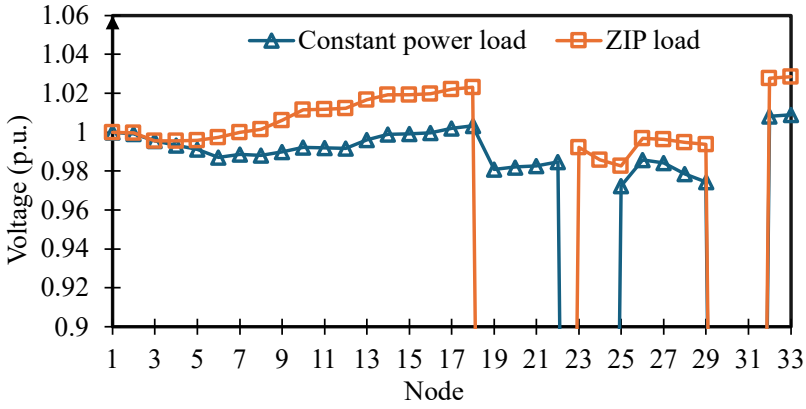

(c) Scenario 3.

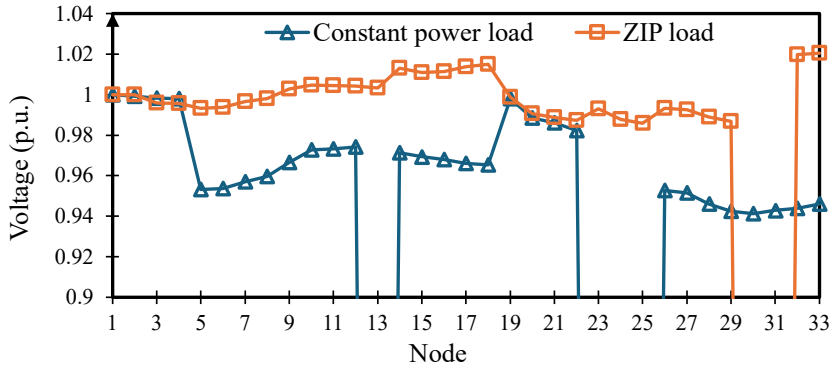

(d) Scenario 4.

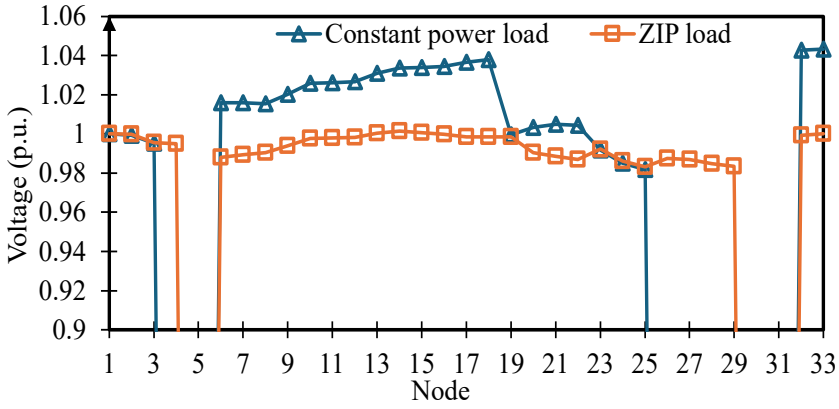

Figure 8. Voltage profile of 33-node grid considering the impact of different load models.

3.2. Vietnamese realistic 190-node distribution system

3.2.1. Data description

The 190-bus Vietnamese distribution network is illustrated in Figure 9. Five DG units are at buses 10, 22, 110, 148, and 174. The data for these distributed generation units are listed in Table 10. Additionally, the operating voltage is set to 1.0 per unit when the DG units are modeled as PV buses.

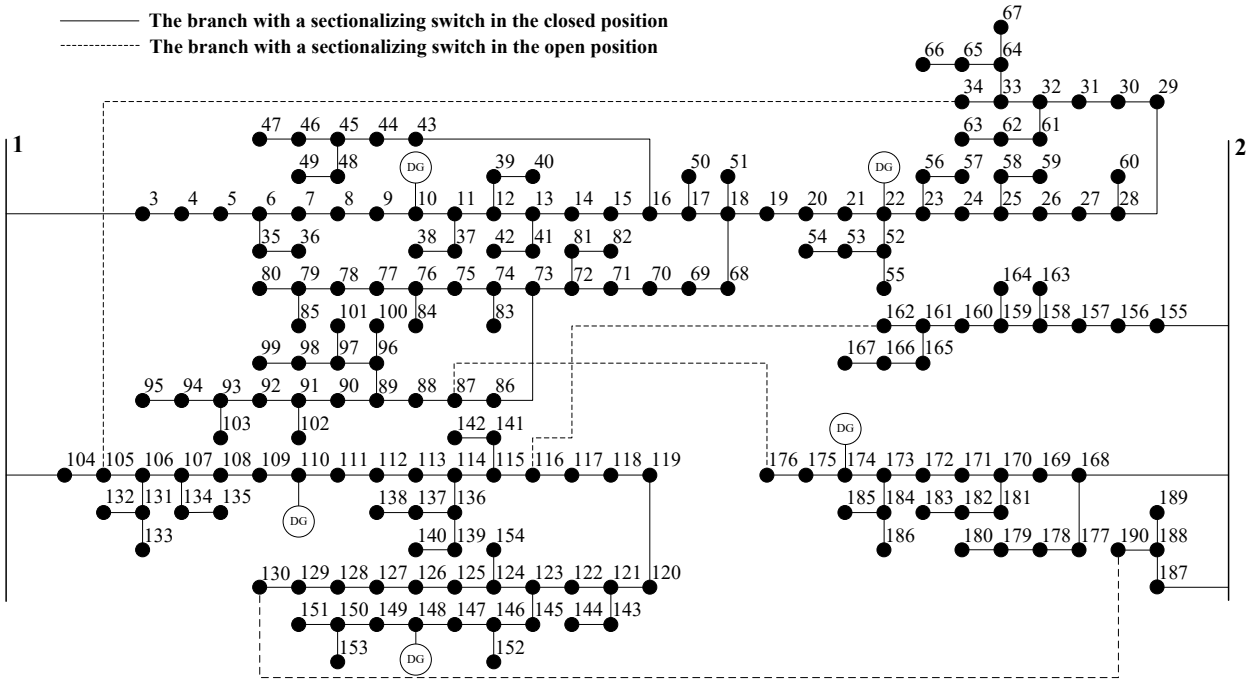

Figure 9. Vietnam 190-bus distribution network.

Table 10. Distributed generation data for the Vietnam 190-bus distribution network.

Location	P_{DG} (kW)	PV Model	
		$\cos\varphi_{DG,leading}$	$\cos\varphi_{DG,lagging}$
10	1000	0.8	0.8
22	1000		
110	1000		
148	1000		
174	1000		

The necessary parameters for distribution network calculations are summarized in Table 11.

Table 11. Technical data of the 190-node Vietnam distribution system.

Parameter	Value
Nominal voltage (kV)	35
Aggregate power of load (MVA)	$26.6734 + j12.9165$
Allowable voltage limits at the nodes (p.u.)	$0.9 \le U \le 1.1$
Allowable current on each branch (kA)	0.273
Base power (MVA)	1
Base voltage (kV)	35

The three types of loads considered in this section are residential loads, service loads, and industrial loads, with the corresponding load types at each bus presented in Table 12. The coefficients of the model of ZIP load corresponding to each load type in the per-unit system [3] are as follows:

- Residential: $a_i^{\mathrm{P}} = 0.24; b_i^{\mathrm{P}} = 0.62; c_i^{\mathrm{P}} = 0.13; a_i^{\mathrm{Q}} = 2.44; b_i^{\mathrm{Q}} = -1.94; c_i^{\mathrm{Q}} = 0.50;$
- Commercial: $a_i^{\mathrm{P}} = 0.16; b_i^{\mathrm{P}} = 0.80; c_i^{\mathrm{P}} = 0.04; a_i^{\mathrm{Q}} = 3.26; b_i^{\mathrm{Q}} = -3.10; c_i^{\mathrm{Q}} = 0.84;$
- Industrial: $a_i^{\mathrm{P}} = -0.07; b_i^{\mathrm{P}} = 0.24; c_i^{\mathrm{P}} = 0.83; a_i^{\mathrm{Q}} = 1.00; b_i^{\mathrm{Q}} = 0; c_i^{\mathrm{Q}} = 0.$

Table 12. Load characteristics of the Vietnamese 190-node distribution network.

Load	Node
Residential	3–30, 161–190
Commercial	31–90, 151–160
Industrial	91–150

Table 13 provides information on the priority levels of the loads. The optimal restoration model for the distribution network after faults is calculated and compared on the Vietnamese 190-bus distribution network under three fault location scenarios, specifically:

- Scenario 1: Fault on the line branch 17–18;
- Scenario 2: Fault on the line branch 160–161;
- Scenario 3: Fault on the line branches 11–12 and 172–173.

Table 13. Load priority levels of the Vietnamese 190-node distribution network

Priority Level	Node
1	3–10, 31–50, 91–110, 151–160
2	11–20, 51–70, 111–130, 161–170
3	21–30, 71–90, 131–150, 171–190

3.2.2. Impact of the objective function

In this section, we describe the impact of different objective functions on the optimal configuration of the distribution network after a fault, considering three objective functions as follows:

- Objective function f_1: Minimizing the total load power not restored, taking into account the priority levels of the loads.
- Objective function f_2: Reducing the overall count of sectionalizing switch actuations.
- Objective functions f_1 and f_2: Combining both objectives using the Pareto optimality.

After performing calculations using the GAMS programming software, the collection of Pareto-efficient outcomes (also known as the Pareto front) for fault scenario 3 is illustrated in Figure 10. According to the formulas described in Eqs (46) and (47), the balanced Pareto optimal solution for the fault at branch 17–18 is identified with a load power loss of 0.0019%, corresponding to 4 switching operations; for the fault at branch 160–161, the load power loss is 0.2656% with 2 switching operations; and for simultaneous faults at branches 11–12 and 172–173, the load power loss is 14.7947% with 8 switching operations.

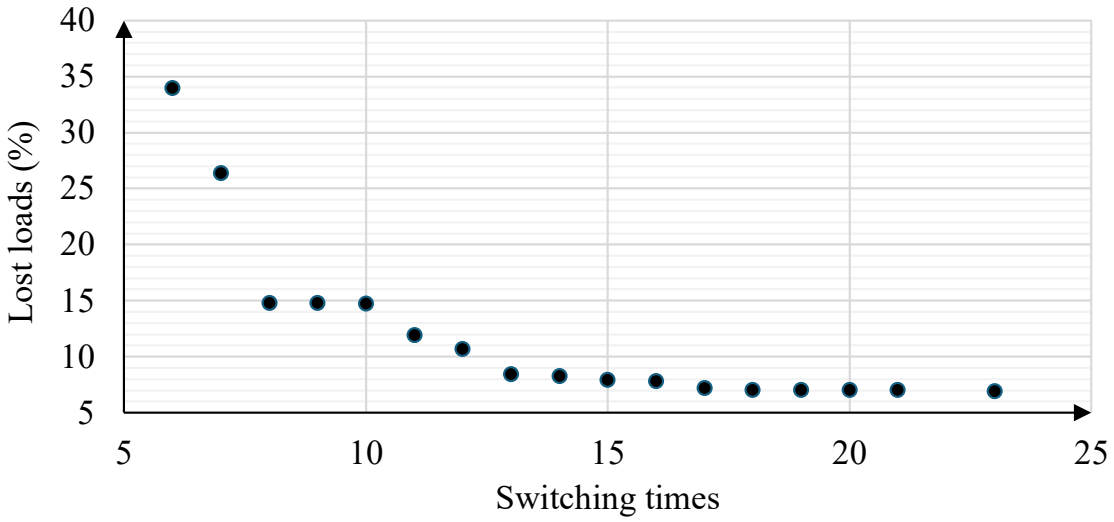

Figure 10. Pareto front of fault Scenario 3 for 190-node test system.

The optimal results of the problem using individual objective functions and the combined objective function (corresponding to the balanced Pareto solutions) for the fault scenarios are presented in Table 14.

The outcomes from Table 14 indicate that the objective function has a significant impact on the optimal structure of the post-fault power grid. Specifically, when optimizing solely for the objective function f_1, the grid achieves a very high load restoration rate in most scenarios; however, this requires a large number of switching operations. In contrast, optimizing for the objective function f_2 significantly reduces the number of operations but severely compromises the load restoration capability. When applying the combined objective function $\{f_1, f_2\}$, the results achieve a balance between the two criteria: The load restoration rate is significantly improved compared to optimizing with f_2, while the number of switching actions is notably decreased compared to optimizing with f_1. This demonstrates the effectiveness and practicality of the multi-objective optimization method in the problem of post-fault distribution system restoration.

Table 14. Impact of objective functions on the 190-bus Vietnamese distribution network.

Scenario	Objective Function	The status of the sectionalizing devices changed after the fault		Number of sectionalizing device switching operations	Total percentage of load power not restored (%)
		Closed sectionalizing device	Open sectionalizing device		
1	f_1	34–105; 87–176; 116–162; 130–190	25–26; 116–117; 158–159	7	0
	f_2	87–176	32–61	2	0.14
	$\{f_1, f_2\}$	34–105; 87–176	25–26; 26–27	4	0.0019
2	f_1	34–105; 87–176; 116–162; 130–190	20–21; 72–73; 120–121	7	0
	f_2	/	87–88	1	14.91
	$\{f_1, f_2\}$	/	72–81; 76–77	2	0.2656
3	f_1	34–105; 87–176; 116–162; 130–190	18–51; 23–56; 25–58; 28–60; 32–61; 52–55; 53–54; 64–65; 64–67; 72–81; 74–75; 74–83; 94–95; 97–101; 98–99; 105–106; 118–119; 184–185; 184–186	23	6.92
	f_2	34–105;87–176	17–18; 76–77; 87–88; 123–124	6	43.31
	$\{f_1, f_2\}$	34–105; 87–176; 130–190	73–74;81–82; 87–88;105–106; 106–107	8	14.7947

3.2.3. Impact of load model

In this section, we indicate the impact of the load model on the optimal grid structure of the distribution network after a fault. The optimization model employs two simultaneous objective functions $\{f_1, f_2\}$. Two load models are considered: The constant power load model (constant P load) and the voltage-dependent load model (ZIP load). DGs are modeled as PV nodes and included in the

calculations. The optimal solution of the problem (corresponding to the balanced Pareto-optimal solution determined according to Eqs (46) and (47)) is presented in Table 15.

Table 15. Impact of load models on the grid structure of the Vietnamese 190-bus network.

Scenario	Load Model	Status of sectionalizing devices after the fault		Number of switching operations of sectionalizing devices	Total disconnected load (%)
		Closed sectionalizing device	Open sectionalizing device		
1	Constant power load	87–176	33–64; 75–76	3	0.2579
	ZIP load	34–105; 87–176	25–26; 26–27	4	0.0019
2	Constant power load	87–176	70–71; 71–72	3	0.2398
	ZIP load	/	72–81; 76–77	2	0.2656
3	Constant power load	34–105;87–176; 116–162	17–50; 22–52; 23–56; 72–81; 73–74; 87–88; 105–106; 106–107; 173–184	12	17.4475
	ZIP load	34–105;87–176; 130–190	73–74;81–82; 87–88; 105–106; 106–107	8	14.7947

The calculation results in Table 15 show a difference between load models in determining the optimal operating structure of the distribution network after a fault, the number of switching operations of sectionalizing devices, and the total load not restored. In Scenario 1, the percentage of load not restored decreases from 0.2579% (constant power load model) to 0.0019% (ZIP load model), while the number of switching operations increases correspondingly from 3 to 4. Conversely, in Scenario 2, the load not restored for the constant power load model (0.2398%) is lower than that of the ZIP load model (0.2656%), and the total number of switching operations decreases correspondingly from 3 to 2. In Scenario 3, the load not restored decreases from 17.4475% (constant power load) to 14.7947% (ZIP load), the count of switching actions decreased from 12 to 8.

Additionally, the voltage profile of the grid under the three fault scenarios, applying two load models, fixed-power load model (constant P load) and voltage-dependent load model (ZIP load), is presented in Figure 11. Analysis of these graphs reveals that the voltage at the nodes tends to decrease progressively as the distance from the source increases. Moreover, changes in the load model affect the node voltage profile in each scenario.

- In Scenario 1, the constant power load model has a lowest voltage of 0.90002 per unit (at node 63), and 11 nodes are not restored with a power supply. Moreover, the ZIP load model has a minimum voltage of 0.9076 per unit (at node 130), but only 1 node is not restored with a power supply.
- In Scenario 2, the lowest voltages are 0.90087 per unit (constant power load) and 0.9016 per unit (ZIP load), both at node 130. However, the constant power load model has 5 nodes without power restoration, compared to 12 nodes without power restoration when using the ZIP load model.
- In Scenario 3, the minimum voltages are 0.90001 per unit using the fixed-power load model and 0.90002 p.u. using the ZIP load model, both occurring at node 40. However, the ZIP load

model has 31 nodes without power restoration compared to 42 nodes without power restoration when using the constant power load model.

(a) Scenario 1.

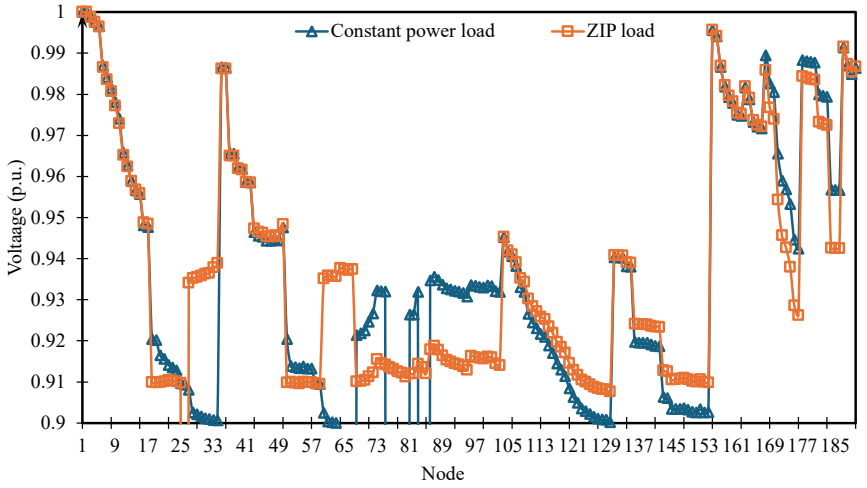

(b) Scenario 2.

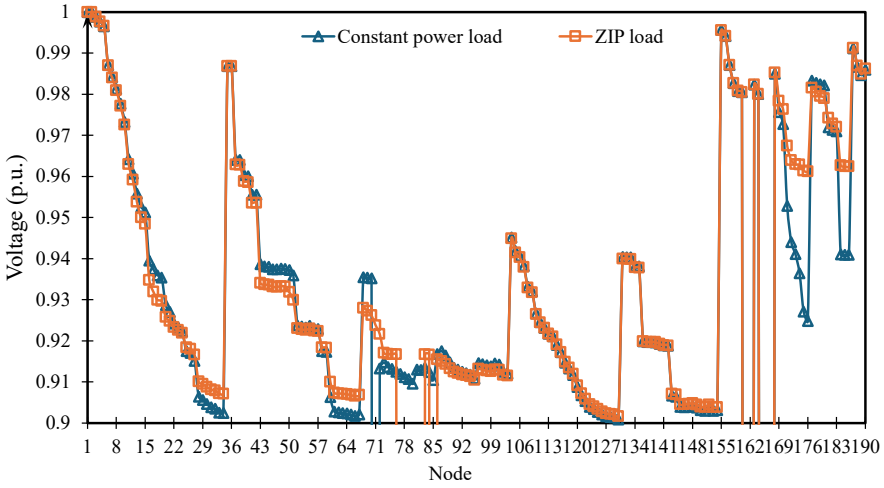

(c) Scenario 3.

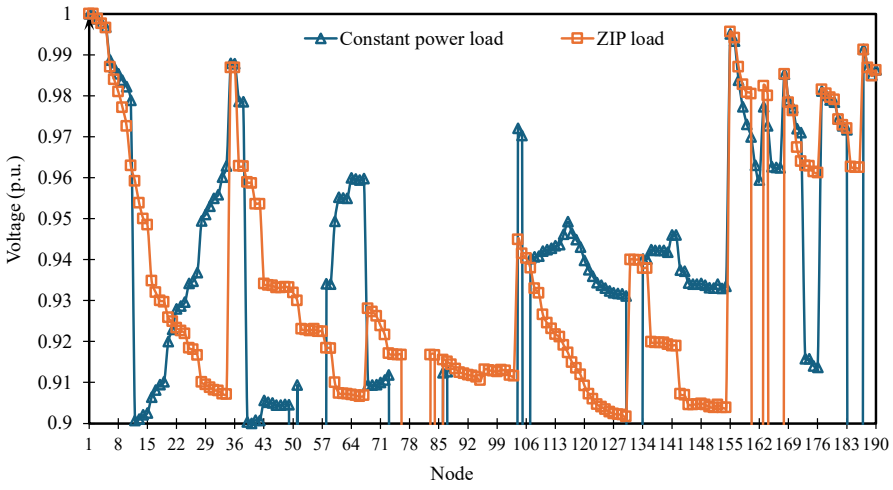

Figure 11. Voltage profile of the 190-bus system considering the impact of different load models.

3.3. Discussion on computation time

Table 16 presents the computation time for the 33-node test system under various fault scenarios. The results show that the computation time is highly dependent on the chosen objective function. Single-objective problems, which aim to minimize either unsupplied load power or total switching operations, require less time to solve than the multi-objective problem. As expected, the combination of two objective functions to find the Pareto front consistently demands the longest computation time, with a maximum of 5.1 s for the fault at Node 5.

Table 16. Computation time (s) for the 33-node test system.

Fault scenario	Objective function		
	Minimization of unsupplied load power	Minimization of total switching operations	Combination of two objective functions to find the Pareto front[1]
Branch 2–3	2.2	1.9	4.1
Branch 2–19	1.8	1.6	3.5
Branches 4–5 and 13–14	2.5	2.1	4.5
Node 5	2.7	2.3	5.1

Likewise, Table 17 presents the computation time for the 190-node test system under various fault scenarios. A trend emerges from the data: The single-objective problems, which aim to minimize either unsupplied load power or total switching operations, require less time to solve than the multi-objective problem. As expected, the combination of two objective functions to find the Pareto front consistently demands the longest computation time, with a maximum of 18.9 s for the fault on branches 11–12 and 172–173.

Table 17. Computation time (s) for the 190-node test system.

Fault scenario	Objective function		
	Minimization of unsupplied load power	Minimization of total switching operations	Combination of two objective functions to find the Pareto front[1]
Branch 17–18	7.9	7.3	15.2
Branch 160–161	6.7	6.4	13.3
Branches 11–12 and 172–173	9.8	9.1	18.9

The consistently low computation times across the small-scale (33-node) and large-scale (190-node) test systems demonstrate the scalability and computational efficiency of the proposed optimization model, making it a viable tool for practical application in real-world distribution networks. Notably, in a practical implementation, the total service restoration time consists of three components: Calculation time, switching action time, and communication time. The communication time from the control system to the terminal is typically less than 10 s, while the switching action time is less than 0.04 s [1].

4. Conclusions

This research presents an optimization problem involving MISOCP-based multi-objective optimization model to address the distribution network restoration problem after faults, with the integration of DG and consideration of voltage-dependent load modeling. The model is formulated with two objective functions: Minimizing the total amount of unsupplied load, taking into account load priority levels, and minimizing the total number of switching operations. The proposed method is tested on the modified IEEE 33-bus distribution system and a real 190-node distribution system in Vietnam under three fault location scenarios. The outcomes demonstrate that the introduced multi-objective optimization technique not only ensures computational efficiency but also meets practical requirements in post-fault distribution network restoration. The analysis of balanced Pareto-optimal solutions reveals a trade-off between the two objectives, thereby supporting decision-making in operational planning aligned with real-world conditions. The application of the MISOCP model not only improves the effectiveness of network restoration but also ensures that the distribution system's radial configuration is preserved while fulfilling technical constraints such as nodal limitations of voltage and branch power flows. Moreover, the proposed optimization approach shows flexibility and adaptability across systems of varying scale and structure, from standard test networks to real-world grids in Vietnam. Additionally, the ZIP load model significantly influences the optimal network operation structure, highlighting the importance of appropriate load modeling in optimization problems.

In future work, we will focus on extending the proposed MISOCP model in several key directions. The framework can be expanded to a multi-period restoration problem, thereby enhancing the performance and reliability of post-fault networks by accounting for time accumulation and incorporating devices like voltage regulation devices and energy storage systems. Additionally, the Pareto front approach can be extended to problems with three or more objectives to assess its scalability and generalizability to higher-dimensional optimization scenarios. A key direction for future work is also to develop more novel computational techniques to address the complexity of network reconfiguration, thereby enhancing the solution efficiency and scalability of the MISOCP approach for large-scale systems.

Use of AI tools declaration

The authors declare they have not used Artificial Intelligence (AI) tools in the creation of this article.

Conflict of interests

The authors declare no conflict of interest.

Author contributions

Conceptualization, Nang-Van Pham; methodology, Nang-Van Pham; software, Trong-Sang Vo and Trung-Hai Nguyen; validation, Trong-Sang Vo and Trung-Hai Nguyen; formal analysis, Trong-Sang Vo and Trung-Hai Nguyen; investigation, Trong-Sang Vo and Trung-Hai Nguyen; resources, Trong-Sang Vo and Trung-Hai Nguyen; data curation, Trong-Sang Vo and Trung-Hai

Nguyen; writing—original draft preparation, Trong-Sang Vo, Trung-Hai Nguyen and Dinh-Phu Vu; writing—review and editing, Nang-Van Pham; visualization, Trong-Sang Vo and Trung-Hai Nguyen; supervision, Nang-Van Pham; project administration, Nang-Van Pham. Ultimately, all of the authors declared no conflicts of interest, contributed to the work, and approved the version that was submitted.

Appendix

Data of branches and load power for the real Vietnamese 190-node test system.

Start node	End node	R (Ω)	X (Ω)	Load at end node	
				P (kW)	Q (kVAr)
1	3	0.0422	0.0420	405	196.1
3	4	0.0422	0.0420	129.6	62.8
4	5	0.0422	0.0420	291.6	141.2
5	6	0.3801	0.3780	0	0
6	7	0.1267	0.1260	81	39.2
7	8	0.1267	0.1260	453.6	219.6
8	9	0.1689	0.1680	145.8	70.6
9	10	0.2112	0.2100	145.8	70.6
10	11	0.3801	0.3780	0	0
11	12	0.1689	0.1680	0	0
12	13	0.2534	0.2520	0	0
13	14	0.2112	0.2100	60.75	29.4
14	15	0.0845	0.0840	0	0
15	16	0.7601	0.7560	0	0
16	17	0.1943	0.1932	0	0
17	18	0.1436	0.1428	0	0
18	19	0.0760	0.0756	145.8	70.6
19	20	0.9713	0.9660	145.8	70.6
20	21	0.2745	0.2730	60.75	29.4
21	22	0.4645	0.4620	0	0
22	23	0.1056	0.1050	0	0
23	24	0.1267	0.1260	81	39.2
24	25	0.6335	0.6300	0	0
25	26	0.0760	0.0756	0	0
26	27	0.2745	0.2730	259.2	125.5
27	28	14.781	14.700	145.8	70.6
28	29	0.1689	0.1680	60.75	29.4
29	30	0.2112	0.2100	60.75	29.4
30	31	0.1900	0.1890	202.5	98.1
31	32	0.0845	0.0840	0	0
32	33	0.3801	0.3780	0	0
33	34	0.2112	0.2100	202.5	98.1
6	35	0.1689	0.1680	145.8	70.6

Continued on next page

Start node	End node	R (Ω)	X (Ω)	Load at end node	
				P (kW)	Q (kVAr)
35	36	0.0422	0.0420	202.5	98.1
11	37	0.0422	0.0420	453.6	219.6
37	38	0.0422	0.0420	453.6	219.6
12	39	0.2196	0.2184	145.8	70.6
39	40	0.2618	0.2604	324	156.9
13	41	0.0845	0.0840	510.3	247.1
41	42	0.0422	0.0420	453.6	219.6
16	43	0.2112	0.2100	145.8	70.6
43	44	0.1267	0.1260	202.5	98.1
44	45	0.0422	0.0420	0	0
45	46	0.3801	0.3780	202.5	98.1
46	47	0.0422	0.0420	202.5	98.1
45	48	0.2534	0.2520	202.5	98.1
48	49	0.2112	0.2100	202.5	98.1
17	50	0.1267	0.1260	259.2	125.5
18	51	0.1689	0.1680	81	39.2
22	52	0.3378	0.3360	0	0
52	53	0.3378	0.3360	0	0
53	54	0.3801	0.3780	202.5	98.1
52	55	0.1689	0.1680	81	39.2
23	56	0.3378	0.3360	145.8	70.6
56	57	0.1267	0.1260	81	39.2
25	58	0.0845	0.0840	81	39.2
58	59	0.9291	0.9240	40.5	19.6
28	60	0.2112	0.2100	145.8	70.6
32	61	0.7179	0.7140	129.6	62.8
61	62	0.2956	0.2940	60.75	29.4
62	63	0.4645	0.4620	81	39.2
33	64	0.1267	0.1260	0	0
64	65	0.2956	0.2940	60.75	29.4
65	66	0.4012	0.3990	202.5	98.1
64	67	0.3378	0.3360	202.5	98.1
18	68	0.2112	0.2100	145.8	70.6
68	69	0.0845	0.0840	145.8	70.6
69	70	0.1267	0.1260	324	156.9
70	71	0.3209	0.3192	81	39.2
71	72	0.2956	0.2940	0	0
72	73	0.6335	0.6300	0	0
73	74	0.2112	0.2100	0	0
74	75	0.0845	0.0840	129.6	62.8
75	76	0.1689	0.1680	0	0

Continued on next page

Start node	End node	R (Ω)	X (Ω)	Load at end node	
				P (kW)	Q (kVAr)
76	77	0.1689	0.1680	60.75	29.4
77	78	0.2323	0.2310	324	156.9
78	79	0.2534	0.2520	0	0
79	80	13.936	13.860	202.5	98.1
72	81	0.1267	0.1260	60.75	29.4
81	82	0.0422	0.0420	526.5	254.9
74	83	0.2534	0.2520	145.8	70.6
76	84	0.1267	0.1260	129.6	62.8
79	85	0.2956	0.2940	202.5	98.1
73	86	0.2534	0.2520	145.8	70.6
86	87	0.0845	0.0840	0	0
87	88	0.1267	0.1260	202.5	98.1
88	89	0.2112	0.2100	0	0
89	90	0.2956	0.2940	81	39.2
90	91	0.1267	0.1260	0	0
91	92	0.2112	0.2100	24.3	11.8
92	93	0.1267	0.1260	0	0
93	94	0.2618	0.2604	60.75	29.4
94	95	0.8024	0.7980	324	156.9
89	96	0.0422	0.0420	0	0
96	97	0.1520	0.1512	0	0
34	105	0.5490	0.5460	0	0
97	98	0.2112	0.2100	81	39.2
98	99	0.2745	0.2730	202.5	98.1
96	100	0.1267	0.1260	324	156.9
97	101	0.1689	0.1680	129.6	62.8
91	102	0.4223	0.4200	324	156.9
93	103	0.4223	0.4200	60.75	29.4
1	104	19.848	19.740	145.8	70.6
104	105	0.1267	0.1260	0	0
105	106	0.0422	0.0420	0	0
106	107	0.0929	0.0924	0	0
107	108	0.2112	0.2100	510.3	247.1
108	109	0.0507	0.0504	324	156.9
109	110	0.2534	0.2520	648	313.8
110	111	0.1056	0.1050	453.6	219.6
111	112	0.0760	0.0756	453.6	219.6
112	113	0.0845	0.0840	145.8	70.6
113	114	0.0422	0.0420	0	0
114	115	0.1985	0.1974	145.8	70.6
115	116	0.2112	0.2100	145.8	70.6

Continued on next page

Start node	End node	R (Ω)	X (Ω)	Load at end node	
				P (kW)	Q (kVAr)
116	117	0.3041	0.3024	81	39.2
117	118	0.1774	0.1764	81	39.2
118	119	0.2112	0.2100	145.8	70.6
119	120	0.4054	0.4032	81	39.2
120	121	0.2956	0.2940	0	0
121	122	0.2323	0.2310	145.8	70.6
122	123	0.2618	0.2604	0	0
123	124	0.1267	0.1260	0	0
124	125	0.1689	0.1680	405	196.1
125	126	0.2534	0.2520	145.8	70.6
126	127	0.2112	0.2100	145.8	70.6
127	128	0.1267	0.1260	145.8	70.6
128	129	0.0422	0.0420	81	39.2
129	130	0.7601	0.7560	202.5	98.1
106	131	0.2956	0.2940	0	0
131	132	0.1689	0.1680	81	39.2
131	133	0.1689	0.1680	145.8	70.6
107	134	0.0422	0.0420	453.6	219.6
134	135	0.0422	0.0420	129.6	62.8
114	136	0.2112	0.2100	0	0
136	137	0.1689	0.1680	81	39.2
137	138	0.0633	0.0630	145.8	70.6
136	139	0.0422	0.0420	453.6	219.6
139	140	0.1267	0.1260	1012.5	490.3
115	141	0.1267	0.1260	145.8	70.6
141	142	0.1267	0.1260	145.8	70.6
121	143	0.0422	0.0420	81	39.2
143	144	0.3801	0.3780	202.5	98.1
123	145	0.0845	0.0840	145.8	70.6
145	146	0.3378	0.3360	0	0
146	147	0.1689	0.1680	202.5	98.1
147	148	0.1267	0.1260	202.5	98.1
148	149	0.1605	0.1596	145.8	70.6
149	150	0.3547	0.3528	0	0
150	151	0.1774	0.1764	259.2	125.5
146	152	0.1267	0.1260	145.8	70.6
150	153	0.2534	0.2520	202.5	98.1
124	154	0.3378	0.3360	202.5	98.1
2	155	0.1689	0.1680	0	0
155	156	0.0633	0.0630	145.8	70.6
156	157	0.3378	0.3360	0	0

Continued on next page

Start node	End node	R (Ω)	X (Ω)	Load at end node	
				P (kW)	Q (kVAr)
157	158	0.2323	0.2310	0	0
158	159	0.1563	0.1554	0	0
159	160	0.1182	0.1176	60.8	29.4
160	161	0.2660	0.2646	0	0
116	162	0.4223	0.4200	81	39.2
161	162	0.1478	0.1470	81	39.2
158	163	0.1267	0.1260	60.8	29.4
159	164	0.2112	0.2100	453.6	219.6
161	165	0.2534	0.2520	145.8	70.6
165	166	0.2112	0.2100	145.8	70.6
166	167	0.2027	0.2016	81	39.2
2	168	0.5068	0.5040	0	0
168	169	0.3801	0.3780	81	39.2
169	170	0.1182	0.1176	0	0
170	171	0.9291	0.9240	202.5	98.1
171	172	0.4223	0.4200	202.5	98.1
172	173	0.1478	0.1470	0	0
173	174	0.2534	0.2520	145.8	70.6
174	175	0.5068	0.5040	81	39.2
87	176	0.4223	0.4200	202.5	98.1
175	176	0.1267	0.1260	202.5	98.1
168	177	0.3801	0.3780	202.5	98.1
177	178	0.1267	0.1260	259.2	125.5
178	179	0.1689	0.1680	202.5	98.1
179	180	0.2112	0.2100	202.5	98.1
170	181	0.3378	0.3360	81	39.2
181	182	0.2787	0.2772	202.5	98.1
182	183	0.3801	0.3780	202.5	98.1
174	184	0.0422	0.0420	0	0
184	185	0.1689	0.1680	129.6	62.8
184	186	0.1689	0.1680	129.6	62.8
2	187	0.4096	0.4074	129.6	62.8
187	188	0.2618	0.2604	0	0
188	189	0.4645	0.4620	259.2	125.5
188	190	0.1267	0.1260	145.8	70.6
130	190	0.5490	0.5460	145.8	70.6

References

1. Li Y, Xiao J, Chen C, et al. (2019) Service restoration model with mixed-integer second-order cone programming for distribution network with distributed generations. *IEEE Trans Smart Grid* 10: 4138–4150. https://doi.org/10.1109/TSG.2018.2850358
2. Zhang Q, Ma Z, Zhu Y, et al. (2021) A two-level simulation-assisted sequential distribution system restoration model with frequency dynamics constraints. *IEEE Trans Smart Grid* 12: 3835–3846. https://doi.org/10.1109/TSG.2021.3088006
3. Marti J, Ahmadi H, Bashualdo L (2013) Linear power flow formulation based on a voltage-dependent load model. *IEEE Trans Power Delivery* 28: 1682–1690. https://doi.org/10.1109/TPWRD.2013.2247068
4. Qian K, Zhou C, Allan M, et al. (2011) Effect of load models on assessment of energy losses in distributed generation planning. *Int J Electr Power Energy Syst* 33: 1243–1250. https://doi.org/10.1016/j.ijepes.2011.04.003
5. Arif A, Wang Z, Wang J, et al. (2018) Load modeling—A review. *IEEE Trans Smart Grid* 9: 5986–5999. https://doi.org/10.1109/TSG.2017.2700436
6. Sekhavatmanesh H, Cherkaoui R (2019) Analytical approach for active distribution network restoration including optimal voltage regulation. *IEEE Trans Power Syst* 34: 1716–1728. https://doi.org/10.1109/TPWRS.2018.2889241
7. Zidan A, Khairalla M, Abdrabou AM, et al. (2017) Fault detection, isolation, and service restoration in distribution systems: state-of-the-art and future trends. *IEEE Trans Smart Grid* 8: 2170–2185. https://doi.org/10.1109/TSG.2016.2517620
8. Abido MA (2006) Multiobjective evolutionary algorithms for electric power dispatch problem. *IEEE Trans Evol Computat* 10: 315–329. https://doi.org/10.1109/TEVC.2005.857073
9. Zitzler E, Thiele L (1999) Multiobjective evolutionary algorithms: a comparative case study and the strength Pareto approach. *IEEE Trans Evol Computat* 3: 257–271. https://doi.org/10.1109/4235.797969
10. Franco JF, Rider MJ, Lavorato M, et al. (2013) Optimal conductor size selection and reconductoring in radial distribution systems using a mixed-integer LP approach. *IEEE Trans Power Syst* 28: 10–20. https://doi.org/10.1109/TPWRS.2012.2201263
11. Chen K, Wu W, Zhang B, et al. (2015) Robust restoration decision-making model for distribution networks based on information gap decision theory. *IEEE Trans Smart Grid* 6: 587–597. https://doi.org/10.1109/TSG.2014.2363100
12. Chen X, Wu W, Zhang B (2016) Robust restoration method for active distribution networks. *IEEE Trans Power Syst* 31: 4005–4015. https://doi.org/10.1109/TPWRS.2015.2503426
13. Chen B, Chen C, Wang J, et al. (2018) Sequential service restoration for unbalanced distribution systems and microgrids. *IEEE Trans Power Syst* 33: 1507–1520. https://doi.org/10.1109/TPWRS.2017.2720122
14. Chen B, Chen C, Wang J, et al. (2018) Multi-time step service restoration for advanced distribution systems and microgrids. *IEEE Trans Smart Grid* 9: 6793–6805. https://doi.org/10.1109/TSG.2017.2723798
15. Sperr F, Stai E, Venkatraman A, et al. (2024) Service restoration in the medium voltage grid minimizing the SAIDI contribution after primary substation failures. *IEEE Trans Power Syst* 39: 66–82. https://doi.org/10.1109/TPWRS.2023.3237976

16. Alizadeh M, Jafari-Nokandi M (2023) A bi-level resilience-oriented islanding framework for an active distribution network incorporating electric vehicles parking lots. *Electr Power Syst Res* 218: 109233. https://doi.org/10.1016/j.epsr.2023.109233
17. Arif A, Wang Z, Wang J, et al. (2018) Power distribution system outage management with co-optimization of repairs, reconfiguration, and DG dispatch. *IEEE Trans Smart Grid* 9: 4109–4118. https://doi.org/10.1109/TSG.2017.2650917
18. Dobson I (2023) Models, metrics, and their formulas for typical electric power system resilience events. *IEEE Trans Power Syst* 38: 5949–5952. https://doi.org/10.1109/TPWRS.2023.3300125
19. Wang F, Chen C, Li C, et al. (2017) A multi-stage restoration method for medium-voltage distribution system with DGs. *IEEE Trans Smart Grid* 8: 2627–2636. https://doi.org/10.1109/TSG.2016.2532348
20. Xu Y, Liu CC, Wang Z, et al. (2019) DGs for service restoration to critical loads in a secondary network. *IEEE Trans Smart Grid* 10: 435–447. https://doi.org/10.1109/TSG.2017.2743158
21. Yang X, Zhou Z, Zhang Y, et al. (2023) Resilience-oriented co-deployment of remote- controlled switches and soft open points in distribution networks. *IEEE Trans Power Syst* 38: 1350–1365. https://doi.org/10.1109/TPWRS.2022.3176024
22. Lei S, Wang J, Hou Y (2018) Remote-controlled switch allocation enabling prompt restoration of distribution systems. *IEEE Trans Power Syst* 33: 3129–3142. https://doi.org/10.1109/TPWRS.2017.2765720
23. Saaklayen MA, Shabbir MNSK, Liang X, et al. (2023) A two-stage multi-scenario optimization method for placement and sizing of soft open points in distribution networks. *IEEE Trans Ind Appl* 59: 2877–2891. https://doi.org/10.1109/TIA.2023.3245588
24. Jiang Y, Jiang J, Zhang Y (2012) A novel fuzzy multiobjective model using adaptive genetic algorithm based on cloud theory for service restoration of shipboard power systems. *IEEE Trans Power Syst* 27: 612–620. https://doi.org/10.1109/TPWRS.2011.2179951
25. Mahdavi M, Alhelou HH, Gopi P, et al. (2023) Importance of radiality constraints formulation in reconfiguration problems. *IEEE Syst J* 17: 6710–6723. https://doi.org/10.1109/JSYST.2023.3283970
26. GAMS Development Corporation. GAMS Documentation, Release 46. Washington, DC: GAMS Development Corporation; 2024. Available from: https://www.gams.com/latest/docs/.
27. Dolatabadi SH, Ghorbanian M, Siano P, et al. (2021) An enhanced IEEE 33 bus benchmark test system for distribution system studies. *IEEE Trans Power Syst* 36: 2565–2572. https://doi.org/10.1109/TPWRS.2020.3038030

AIMS Press